Spectroscopy of ^{20}F levels

S. Raman
Oak Ridge National Laboratory, Oak Ridge, Tennessee 37831

E. K. Warburton*
Brookhaven National Laboratory, Upton, New York 11973

J. W. Starner, E. T. Jurney, and J. E. Lynn
Los Alamos National Laboratory, Los Alamos, New Mexico 87545

P. Tikkanen and J. Keinonen
University of Helsinki, Accelerator Laboratory, FIN-00014 Helsinki, Finland

(Received 4 August 1995)

From a study of the ^{19}F(n,γ) reaction with thermal neutrons incident on a Teflon target, 168 γ rays have been detected and incorporated into a level scheme of ^{20}F consisting of 35 previously known levels and a new one at 5939 keV. Two low-energy primary $E1$ transitions of energies 584 and 665 keV together account for more than half of the total capture cross section. They populate, respectively, states at 6018 and 5936 keV (both $J^{\pi}=2^{-}$). These states are also excited strongly in the ^{19}F(d,p) reaction. From each of these states, 17 γ rays were observed to the lower-lying states. These γ rays constitute the largest number of branches reported from any nuclear bound state. A weak $(6\pm1\,\mu\text{b})\,\gamma$ ray of energy 4630.6 ± 0.9 keV, placed as a transition between the neutron-capturing state (which is a 0^{+} and 1^{+} mixture) and the 1971-keV, (3^{-}) state, might represent the first observation of a primary $M2$ transition in the (n,γ) reaction. The total thermal-neutron-capture cross section of ^{19}F was measured as 9.51 ± 0.09 mb; and the neutron separation energy of ^{20}F as 6601.35 ± 0.04 keV. Estimates of direct neutron capture have been made using physically realistic optical-model parameters. These model estimates are in reasonable agreement with the measured (partial) cross sections. While constructing the (n,γ) level scheme, the existing data on bound levels in ^{20}F were critically evaluated. The lifetime values for many levels are poorly known. Therefore, the lifetimes for 25 levels were measured by the Doppler-shift-attenuation method using the inverse reaction ^{2}H(^{19}F, $p\gamma$) on implanted deuterium targets. The experimental level properties such as excitation energies, J^{π} assignments, branching ratios, and lifetimes have been compared with the results from a large-basis shell-model calculation. The agreement was found to be quite good, but this comparison points out also the need for acquiring new data to give more definitive J^{π} assignments.

PACS number(s): 25.40.Lw, 21.10.Tg, 21.60.Cs, 27.30.+t

I. INTRODUCTION

There is now a substantial body of evidence [1] to show that a simple direct mechanism—consisting of a neutron that is initially in an s orbit in the overall potential field of the target nucleus making a transition to a p-wave orbit in the final nucleus—can explain the absolute cross sections of primary electric-dipole $E1$ transitions in the (n,γ) reaction at off-resonance energies. This is especially the case for light nuclei $(A<50)$. In a series of recent papers [1–8], this mechanism has been employed in the analysis of experimental data in a quantitative way. For all the nuclides studied in these papers, the bulk of the $E1$ primary transitions following thermal-neutron capture can be described as predominantly direct in nature, and the small discrepancies between the quantitative estimate of the direct-capture cross sections (in a realistic optical-model framework) and the experimental data can be attributed plausibly to the admixture of more complex ''compound-nuclear'' contributions to the capture amplitudes.

The case of $^{19}_{9}F_{10}$ is especially interesting for two reasons: (i) This nucleus lies just above the group of nuclides ending with $^{16}_{8}O_{8}$ where the $0p$ shell[1] has become filled, and the $1p$ orbit still lies at higher energy; hence, the single-particle $0p$-wave components are expected to be small in the low-lying final states of ^{20}F, and the competition between the direct and compound-nuclear mechanisms in the ^{19}F(n,γ) reaction may be more severe than in the cases treated before [2–8]. (ii) Partially reflecting this expected lack of $0p$-wave content, the bulk of the capture cross section is carried by two comparatively low-energy transitions ($\sim$ 0.6 MeV) in contrast to the capture spectra of most nuclides in which the strongest primary transitions are at much higher energies. Our objective is to ascertain if the overall (n,γ) behavior of ^{19}F is consistent with our current understanding and knowledge of the capture mechanisms.

*Deceased.

[1]Our notation $N=0,1,2,\ldots$ for the principal quantum number is different from $N=1,2,3,\ldots$ that we used earlier [2–8]. The current notation seems preferable because (i) N directly gives the number of nodes in the radial wave function and (ii) $2N+l$ gives the number of quanta in the major oscillator orbit.

TABLE I. Partial list of references to previous measurements on ^{20}Fe levels. See Ref. [9] for additional references.

Measurement	Author(s)	Year	Facility[a]	Reference
^{11}B(^{13}C,α) reaction	Liu and Fortune	1988	U. Penn.	[10]
^{11}B(^{13}C,$\alpha\gamma$) reaction	Legg *et al.*	1978	U. Penn.	[11]
^{13}C(^{11}B,α) reaction	Liu and Fortune	1988	U. Penn.	[10]
^{14}N(^{7}Li,p) reaction	Fortune and Bishop	1977	U. Penn.	[12]
	Fortune and Eckman	1985	U. Penn.	[13]
^{16}O(^{7}Li,^{3}He) reaction	Fortune and Bishop	1978	U. Penn.	[14]
^{18}O(^{3}He,p) reaction	Rollefson, Jones, and Shea	1970	U. Notre Dame	[15]
	Fortune *et al.*	1971	U. Penn.	[16]
	Crozier and Fortune	1974	U. Penn.	[17]
	Medoff *et al.*	1976	U. Penn.	[18]
	Chowdhury, Zaman, and Sen Gupta	1992	Oxford U.	[19]
^{18}O(^{3}He,$p\gamma$) reaction	Bissinger *et al.*	1967	U. Notre Dame	[20]
	Quin *et al.*	1967	U. Notre Dame	[21]
	Quin, Bissinger, and Chagnon	1970	U. Notre Dame	[22]
	Alexander *et al.*	1972	U. Notre Dame	[23]
	Longo *et al.*	1973	U. Notre Dame	[24]
	Pronko	1973	Lockheed	[25]
	Balamuth and Adelberger	1977	U. Penn.	[26]
^{18}O(t,$n\gamma$) reaction	Pronko and Nightingale	1971	Lockheed	[27]
	Pronko	1973	Lockheed	[25]
^{19}F(thermal n,γ) reaction	Spilling *et al.*	1968	Petten	[28]
	Hardell and Hasselgren	1969	Stockholm	[29]
	Hungerford *et al.*	1983	Grenoble	[30]
	Kennett, Prestwich, and Tsai	1987	McMaster U.	[31]
^{19}F(resonance n,γ) reaction	Bergqvist *et al.*	1967	Oak Ridge	[32]
	Kenny *et al.*	1974	Lucas Heights	[33]
^{19}F(d,p) reaction	Rollefson, Jones, and Shea	1970	U. Notre Dame	[15]
	Rollefson and Aymar	1971	U. Notre Dame	[34]
	Fortune *et al.*	1971	U. Penn.	[16]
	Fortune *et al.*	1972	U. Penn.	[35]
	Fortune and Betts	1974	U. Penn.	[36]
	Mosley and Fortune	1977	U. Penn.	[37]
^{19}F(polarized d,p) reaction	Quin and Vigdor	1970	U. Notre Dame	[38]
^{19}F(d,$p\gamma$) reaction	Chagnon	1964	U. Notre Dame	[39]
	Newsome	1965	U. Michigan	[40]
	Hershberger, Wozniak, and Donahue	1969	U. Arizona	[41]
	Holtebekk, Tryti, and Vamraak	1969	U. Oslo	[42]
	Hardy and Lee	1973	Johns Hopkins U.	[43]
^{20}O β^- decay	Scharff-Goldhaber, Goodman, and Silbert	1960	Brookhaven	[44]
	Freiberg and Soergel	1966	U. Freiburg	[45]
	Alburger, Wang, and Warburton	1987	Brookhaven	[46]
^{20}Ne(t,^{3}He) reaction	Clarke *et al.*	1990	Daresbury	[47]
^{21}Ne(d,^{3}He) reaction	Millington *et al.*	1974	Chalk River	[48]
^{21}Ne(t,α) reaction	Liu and Fortune	1988	U. Penn.	[49]
^{22}Ne(d,α) reaction	Fortune and Garrett	1976	U. Penn.	[50]
Lifetimes	Nickles	1969	U. Wisconsin	[51]
(See also Tables VII and VIII)	Hershberger, Wozniak, and Donahue	1969	U. Arizona	[41]
	Holtebekk, Strømme, and Tryti	1970	U. Oslo	[52]
	Pronko and Nightingale	1971	Lockheed	[27]
	Pronko	1973	Lockheed	[25]
	Warburton *et al.*	1973	Brookhaven	[53]
	Warburton, Gorodetzky, and Becker	1973	Brookhaven	[54]
	Seiler *et al.*	1975	ETH Zurich	[55]
	Kozub *et al.*	1983	Brookhaven	[56]
	Görres *et al.*	1994	U. Notre Dame	[57]

[a]Facility where the actual measurements were done. The symbol U stands for a university.

Approximately 88 bound states are known in ^{20}F from a variety of studies (see Table I) [9–57]. About 40% of these are populated significantly in the current (thermal n,γ) study. In this paper, we have provided a conspectus of these bound states, their spin and parity (J^{π}) assignments, and the reasons for these assignments. We have surveyed the lifetimes of these bound states by the Doppler-shift-attenuation (DSA) method using the inverse reaction ^{2}H(^{19}F, $p\gamma$) on deuterium targets implanted in gold (high stopping power) and silicon (low stopping power) backings. Computer simulations of the γ-ray line shapes with the Monte Carlo (MC) method have yielded lifetime values for 25 bound states below an excitation energy of 6.1 MeV. We have also compared the level properties of ^{20}F with those calculated with a large-basis shell-model interaction.

II. MEASUREMENTS AND RESULTS

A. Gamma rays in ^{20}F

The ^{19}F(n,γ) reaction with thermal neutrons has been studied previously with Ge detectors at the Petten, Stockholm, Grenoble, and McMaster reactors by Spilling *et al.* [28], Hardell and Hasselgren [29], Hungerford *et al.* [30], and Kennett, Prestwich, and Tsai [31], respectively. The Petten, Stockholm, and McMaster studies employed Teflon $[(C_2F_2)_n]$ targets that can be obtained readily in an ultrapure form—a factor that is important given the small cross section for this reaction ($\sim$10 mb). (Among natural elements, only He, Be, C, O, and Ne have cross sections that are smaller.) At the Grenoble high-flux reactor, Hungerford *et al.* [30] chose not to use Teflon, probably fearing decomposition resulting from heating of the sample. Instead, they employed targets of NaF and PbF_2, and relied, for proper identification as a γ ray in ^{20}F, on its appearance in both spectra with the correct intensity ratio.

In this work, the ^{19}F(n,γ) reaction was studied with a 4.30-g Teflon target placed in the thermal column of the internal target facility at the 8-MW Los Alamos Omega West Reactor. This facility and the data analysis procedures have been described in detail in Refs. [2] and [6]. The neutron flux at the target position was $\sim 6\times 10^{11}$ n/cm^2 s. This flux was approximately Maxwellian corresponding to a temperature of 350 K. Gamma-ray spectra were obtained with a 30-cm^3 coaxial intrinsic Ge detector positioned inside a 20-cm-diam $\times$ 30-cm-long NaI(Tl) annulus. The Ge detector was operated either in the Compton-suppressed mode (with a gain of 0.453 keV/channel) or in the pair-spectrometer mode (0.628 keV/channel). Selected portions of the measured spectra are shown in Fig. 1.

The primary calibration energies were those recommended by Wapstra [58]: 511.000 $\pm$ 0.002 keV for annihilation radiation; 2223.253 $\pm$ 0.004 keV for the γ ray from the ^{1}H(n,γ) reaction, and 4945.303 $\pm$ 0.030 keV for the ground-state transition in the ^{12}C(n,γ) reaction. All capture cross sections reported herein are normalized to the recommended value of $\sigma_{\gamma}(2200\ \mathrm{m/s}) = 332.6 \pm 0.7$ mb [59] for ^{1}H present in a 100.0-mg CH_2 standard. Because the most probable neutron velocity v was greater than 2200 m/s, a $1/v$ dependence was assumed for the capture cross sections of both ^{1}H and ^{19}F. Corrections for self-absorption and attenuation were applied. The γ-ray energies (E_{γ}), intensities (I_{γ}), and level placements are listed in Table II.

Many doublets ($\sim$20 with separation $<$4 keV) were present in the spectra. Through optimization and gain stabilization, performance levels [as measured by the full width at half maximum (FWHM)] in the Compton-suppressed mode of 1.33, 1.71, 2.27, and 2.69 keV were attained for γ rays of energies 0.5, 1.0, 2.0, and 3.0 MeV, respectively. In the pair-spectrometer mode, the FWHM values were 1.82, 2.76, 3.10, and 3.49 keV for γ rays of energies 2, 4, 5, and 6 MeV, respectively. The ability to visualize the 3586.2- and 3589.5-keV doublet [see Fig. 1(c)] and the 4092.3- and 4095.0-keV doublet [see Fig. 1(d)] are examples of the resolution capabilities of this system. At 5 MeV, the current FWHM of 3.10 keV compares favorably with the previous best value of 3.7 keV attained at McMaster [31].

The 3098-keV and the 4070-keV peaks in Fig. 1(b) and Fig. 1(d), respectively, represent very weak (~ 7 μb each) γ rays. The detection limit for a γ ray in the 0.1–10.0 MeV region was typically $\sim$3 photons per 10^4 thermal-neutron captures (or ~ 3 μb) which is a factor of $\sim$2 better than in previous measurements. This improvement, in turn, has resulted in a significant increase (see Table III) in the number of γ rays (particularly below 3 MeV) identified in this work as belonging to ^{20}F. Most of the 24 unplaced γ rays and a few of the placed γ rays reported by Hungerford *et al.* [30] were found to be spurious. However, their origins could not all be traced. The remaining 89 γ rays listed by them and all γ rays (totaling 91) assigned to ^{20}F by Kennett, Prestwich, and Tsai [31] have been confirmed in this work.

The peak at 662 keV [see Fig. 1(a)], which has been treated in all previous studies [28–31] as representing a single transition between levels at 1971 and 1309 keV, is actually a very close doublet. If analyzed as a single peak, the measured energy of 661.86 $\pm$ 0.03 keV differs significantly from the value of 661.63 $\pm$ 0.04 keV expected for the 1971 $\rightarrow$ 1309 keV transition from energy combinations involving other transitions. Once the lower member of the doublet is *fixed* at 661.63 keV, the analysis [see Fig. 1(a)] reveals the presence of a weak 662.2-keV γ ray between the stronger 661.6- and 665.2-keV γ rays.

B. Level scheme of ^{20}F

The level scheme resulting from this work is presented in Table IV. All γ rays (except for three weak ones at 804, 1035, and 3917 keV) have been incorporated into this scheme consisting of 36 bound states. By combining the results of the four previous (n,γ) studies [28–31], it is possible to make a list of 29 levels that are populated significantly in this reaction. Of these, 26 are genuine including the levels at 3590 and 4592 keV proposed by Kennett, Prestwich, and Tsai [31]. The levels proposed at 4508.7 keV by Hungerford *et al.* [30] at 5413.1 keV by Spilling *et al.* [28], and at 5713 keV by Hardell and Hasselgren [29] are most probably not genuine. The γ rays associated with these levels are either not seen in the current, more sensitive study or are placed elsewhere in the level scheme. A new level has been introduced at 5939 keV that is populated mainly by the 662.2-keV γ ray. This level deexcites by means of five secondary γ rays. Except for this level, all other levels deduced

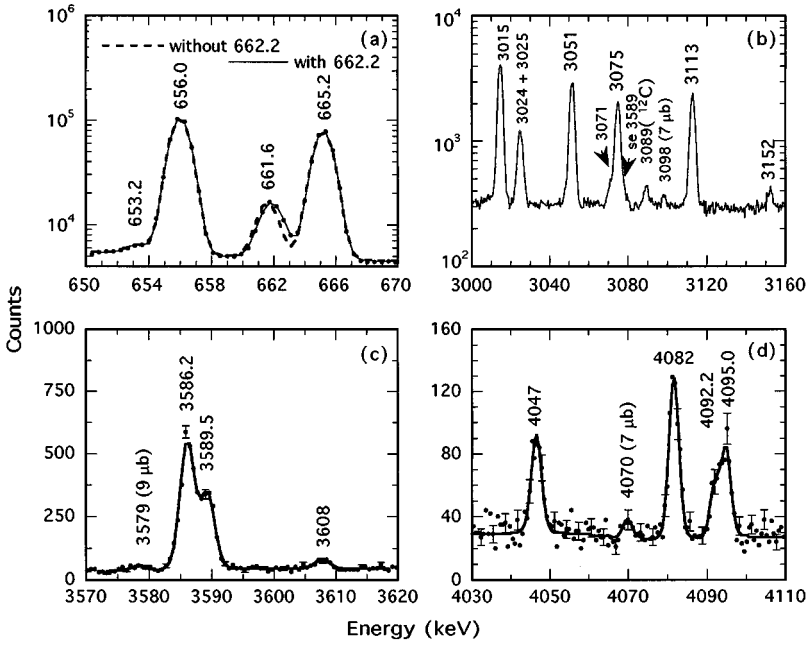

FIG. 1. Portions of the γ-ray spectrum from the ^{19}F$(n,\gamma)^{20}$F reaction with thermal neutrons showing several resolved doublets. See Sec. II A for related discussion.

from the current experiment correspond to known levels in ^{20}F. The population in the (n,γ) reaction of the known levels at 2865, 3172, 4893, 5226, 5283, 5466, 5623, 5810, and 6299 keV is reported here for the first time.

Level energies listed in Table IV from this work were obtained through an overall least-squares fit involving all placed transitions except those noted in Table II with a footnote d. In deducing these level energies, nuclear recoil was taken into account. The intensity balance for each of the excited states is excellent (see columns 5–7 of Table IV).

For most states in ^{20}F, the charged-particle reaction study with the smallest reported uncertainties in the quoted level energies is the (d,p) study by Rollefson, Jones, and Shea [15]. Where comparisons can be made, their energies agree very well with the more accurate values obtained in the current (thermal n,γ) study except for some small systematic differences as shown in Fig. 2(a). It is straightforward then to apply a small correction to the (d,p) energies of Ref. [15] [see Fig. 2(b) and Table V]. In constructing the overall level scheme for ^{20}F, given in a later Table IX, we have used the corrected energies for those (d,p) levels not seen in (thermal n,γ).

C. Neutron separation energy

Our deduced neutron separation energy S_n for ^{20}F is 6601.35 $\pm$ 0.04 keV where the uncertainty now includes the uncertainty in the primary calibration energies. Our value and those obtained by earlier workers, 6601.33 $\pm$ 0.14 keV [30] and 6601.36 $\pm$ 0.05 keV [31], are in excellent agreement even though there are small differences between their standards and ours.

D. Capture cross section of ^{19}F

If a level scheme is complete and internal conversion can be neglected, the quantities ΣI_γ (primary), $\Sigma E_\gamma I_\gamma / S_n$, and ΣI_γ (secondary to ground state) should all be the same within their stated uncertainties. In the case of ^{20}F, the measured values (in units of mb) are 9.54 $\pm$ 0.18, 9.53 $\pm$ 0.11, and 9.47 $\pm$ 0.15, respectively. These values also agree with the cross-section value of 9.51$\pm$ 0.09 mb based on the subsequent β^- decay of ^{20}F represented by the 1633.52 $\pm$ 0.03 keV γ ray in ^{20}Ne. Our recommended cross-section value of 9.51 $\pm$ 0.09 mb for the ^{19}F(n,γ) reaction is significantly more precise than the currently accepted value of 9.6 $\pm$ 0.5 mb [59].

E. Gamma-ray branching ratios

The γ-ray branching ratios measured in the current and previous studies are important in determining allowable J^π assignments for the low-lying states (defined here as $<$ 4.0 MeV). We list the known branching ratios for these states in Table VI. With the exception of the 1824-, 2968-, and 3172-keV levels, the listed values are from the current study. The uncertainties in our branching ratios are generally smaller than those of previous determinations. The branching limits for the 1824- and 3172-keV levels are from Refs. [25] and [22], respectively. The results quoted for the 2968-keV level are based on data from Ref. [11], but they are different from the originally published values of 61 $\pm$ 4% and 39 $\pm$ 4% for the 2968 $\rightarrow$ 1971 keV and 2968 $\rightarrow$ 823 keV transitions, respectively, which are based solely on the intensities of these two transitions observed at 90° to the beam direction. Legg *et al.* [11] have also listed intensities for other transitions observed in coincidence with the gate set on the ''2968-keV'' particle group, which gate encompassed as well any formation of the nearby 2966-keV level. Our reinterpretation of these results includes (i) allowance for a possible contribution in the particle gate from the unresolved 2966-keV level (with the branching ratios observed in the current study), (ii) possible angular-correlation effects, and (iii) consideration (besides the two main transitions) of the other observed transitions—but allowing for some background of random coincidences.

TABLE II. Energies (E_γ) and intensities (I_γ) of γ rays from the ^{19}F(thermal, n,γ)^{20}F reaction.

E_γ(keV)[a]	I_γ(mb)[b]	Placement[c]	E_γ(keV)[a]	I_γ(mb)[b]	Placement[c]	E_γ(keV)[a]	I_γ(mb)[b]	Placement[c]
166.78 *5*	0.44 *4*	823 → 656	1853.96 *22*	0.013 *2*	5936 → 4082	2981.25 *18*	0.035 *4*	3965 → 984
252.65 *23*	0.008 *2*	1309 → 1057	1935.50 *5*	0.073 *5*	6018 → 4082	3014.58 *3*	0.405 *16*	C → 3587
302.2 *3*	0.005 *2*	C → 6299	1970.73[d] *4*	0.090 *9*	1971 → 0	3023.90[d] *9*	0.032 *4*	3680 → 656
325.73 *14*	0.041 *3*	1309 → 984	1970.95[d] *5*	0.010 *3*	5936 → 3965	3025.10[d] *4*	0.076 *5*	4082 → 1057
534.60 *8*	0.013 *2*	1844 → 1309	2009.52 *7*	0.047 *4*	C → 4592	3051.43 *4*	0.297 *12*	6018 → 2966
556.41 *3*	0.202 *13*	C → 6045	2038.08 *18*	0.015 *2*	4082 → 2044	3070.9 *3*	0.020 *3*	5936 → 2865
583.55 *3*	3.60 *15*	C → 6018	2042.0 *6*	0.005 *2*	2865 → 823	3074.81 *6*	0.189 *8*	C → 3526
620.44 *5*	0.023 *2*	3587 → 2966	2043.89 *6*	0.068 *5*	2044 → 0	3098.1 *4*	0.007 *2*	4082 → 984
653.2 *3*	0.020 *3*	1309 → 656	2052.8 *6*	0.005 *1*	6018 → 3965	3112.72 *6*	0.240 *9*	C → 3488
656.00 *3*	1.98 *10*	656 → 0	2079.72 *21*	0.011 *2*	6045 → 3965	3152.1 *4*	0.014 *3*	6018 → 2865
661.63[d] *4*	0.151 *20*	1971 → 1309	2120.95 *16*	0.014 *2*	3965 → 1844	3219.89 *12*	0.061 *4*	4277 → 1057
662.24[d] *14*	0.102 *15*	C → 5939	2143.26 *3*	0.196 *9*	2966 → 823	3293.23 *22*	0.026 *3*	4277 → 984
665.21 *3*	1.49 *8*	C → 5936	2179.09 *4*	0.091 *6*	3488 → 1309	3387.56 *11*	0.061 *5*	4371 → 984
670.1 *6*	0.003 *1*	2865 → 2194	2187.96 *20*	0.013 *2*	3172 → 984	3475.3 *4*	0.005 *1*	5319 → 1844
691.4 *3*	0.004 *2*	4371 → 3680	2194.16 *3*	0.133 *6*	2194 → 0	3488.13 *4*	0.72 *3*	3488 → 0
734.84 *12*	0.006 *2*	2044 → 1309	2208.5 *7*	0.002 *1*	2865 → 656	3534.4 *4*	0.014 *3*	4592 → 1057
771.71 *10*	0.008 *2*	2966 → 2194	2229.8 *4*	0.052 *5*	C → 4371	3578.6 *5*	0.009 *2*	5623 → 2044
791.2 *4*	0.004 *1*	C → 5810	2232.9 *9*	0.021 *3*	4277 → 2044	3586.23 *6*	0.290 *12*	3587 → 0
793.36 *19*	0.007 *2*	3965 → 3172	2255.82 *4*	0.087 *5*	5936 → 3680	3589.47 *8*	0.178 *7*	3590 → 0
803.65 *11*	0.009 *2*	unplaced	2309.96 *6*	0.041 *4*	2966 → 656	3607.8 *3*	0.021 *3*	4592 → 984
820.9 *4*	0.005 *2*	2865 → 2044	2324.11 *3*	0.117 *5*	C → 4277	3679.91 *23*	0.087 *6*	3680 → 0
822.69 *4*	0.219 *12*	823 → 0	2337.58 *14*	0.014 *3*	6018 → 3680	3711.0 *5*	0.012 *3*	5555 → 1844
885.0 *3*	0.005 *1*	2194 → 1309	2346.30 *16*	0.021 *4*	5936 → 3590	3741.44 *11*	0.058 *5*	5936 → 2194
894.1 *5*	0.003 *1*	2865 → 1971	2349.55 *13*	0.031 *3*	5936 → 3587	3823.05 *9*	0.106 *6*	6018 → 2194
978.19 *6*	0.061 *10*	C → 5623	2352.44 *21*	0.017 *3*	5939 → 3587	3891.39 *25*	0.018 *3*	5936 → 2044
983.53 *3*	1.16 *6*	984 → 0	2370.88 *21*	0.008 *2*	3680 → 1309	3894.2 *4*	0.012 *3*	5939 → 2044
987.2[e] *4*	0.004 *1*	1971 → 984	2427.83 *4*	0.190 *7*	6018 → 3590	3916.9 *5*	0.008 *3*	unplaced
1020.9 *4*	0.003 *1*	2865 → 1844	2431.08[d] *3*	0.35 *3*	6018 → 3587	3964.85[f] *4*	0.441 *16*	5936 → 1971
1035.0 *3*	0.009 *2*	unplaced	2431.43[d] *3*	0.07 *3*	3488 → 1057	3973.47 *20*	0.024 *3*	6018 → 2044
1046.00 *4*	0.177 *9*	C → 5555	2447.58 *4*	0.141 *7*	5936 → 3488	4009.3 *5*	0.010 *3*	5319 → 1309
1056.78 *3*	0.94 *4*	1057 → 0	2458.0 *4*	0.006 *1*	6045 → 3587	4046.71 *23*	0.036 *3*	6018 → 1971
1135.38 *17*	0.009 *2*	C → 5466	2469.34 *4*	0.197 *8*	3526 → 1057	4070.0 *6*	0.007 *2*	4893 → 823
1148.05 *4*	0.264 *15*	1971 → 823	2504.54 *18*	0.038 *4*	3488 → 984	4081.77 *10*	0.054 *4*	4082 → 0
1187.70 *6*	0.045 *3*	1844 → 656	2519.05 *6*	0.070 *5*	C → 4082	4092.2 *4*	0.017 *3*	5936 → 1844
1282.14 *4*	0.086 *5*	C → 5319	2529.20[d] *3*	0.58 *3*	6018 → 3488	4095.01 *23*	0.028 *3*	5939 → 1844
1306.2 *3*	0.009 *2*	4893 → 3587	2529.55[d] *3*	0.09 *3*	3587 → 1057	4173.54 *5*	0.167 *6*	6018 → 1844
1309.17 *3*	0.76 *3*	1309 → 0	2556.35 *15*	0.016 *3*	6045 → 3488	4200.56 *7*	0.108 *6*	6045 → 1844
1318.52 *10*	0.023 *2*	C → 5283	2600.3 *6*	0.004 *2*	5466 → 2865	4225.8 *7*	0.006 *1*	5283 → 1057
1371.53 *4*	0.145 *9*	2194 → 823	2602.75 *9*	0.035 *3*	3587 → 984	4245.65 *8*	0.093 *5*	5555 → 1309
1375.2 *4*	0.005 *2*	C → 5226	2623.18 *8*	0.044 *3*	3680 → 1057	4262.5 *9*	0.003 *1*	5319 → 1057
1387.90 *3*	0.83 *3*	2044 → 656	2636.11 *5*	0.097 *5*	C → 3965	4313.29 *25*	0.018 *3*	5623 → 1309
1392.22 *5*	0.078 *6*	3587 → 2194	2655.74 *6*	0.078 *6*	3965 → 1309	4335.09 *13*	0.047 *4*	5319 → 984
1542.50 *4*	0.274 *12*	3587 → 2044	2690.5 *3*	0.006 *1*	5555 → 2865	4556.81 *4*	0.522 *20*	C → 2044
1545.87 *16*	0.013 *2*	3590 → 2044	2697.9 *5*	0.004 *1*	4893 → 2194	4626.5[g] *5*	0.008 *2*	5936 → 1309
1555.0 *4*	0.005 *1*	2865 → 1309	2864.68 *13*	0.016 *4*	2865 → 0	4630.6 *9*	0.006 *1*	C → 1971
1644.50 *8*	0.073 *6*	3488 → 1844	2921.01 *8*	0.094 *5*	C → 3680	4639.0 *4*	0.023 *4*	5623 → 984
1708.52 *22*	0.026 *3*	C → 4893	2930.31 *10*	0.086 *5*	3587 → 656	4708.19 *12*	0.052 *4*	6018 → 1309
1742.7 *3*	0.006 *2*	3587 → 1844	2933.76 *25*	0.023 *3*	3590 → 656	4735.22 *10*	0.054 *4*	6045 → 1309
1836.50 *22*	0.016 *2*	3680 → 1844	2965.90 *9*	0.091 *5*	2966 → 0	4757.02 *5*	0.189 *8*	C → 1844
1843.74 *3*	0.61 *3*	1844 → 0	2969.7 *4*	0.016 *3*	5936 → 2966	4878.8 *6*	0.009 *2*	5936 → 1057

TABLE II. (*Continued*).

E_γ(keV)[a]	I_γ(mb)[b]	Placement[c]	E_γ(keV)[a]	I_γ(mb)[b]	Placement[c]	E_γ(keV)[a]	I_γ(mb)[b]	Placement[c]
4899.2 *9*	0.007 *2*	5555 → 656	5282.1 *6*	0.008 *2*	5283 → 0	5616.82 *7*	0.138 *6*	C → 984
4951.91 *25*	0.059 *6*	5936 → 984	5291.40 *6*	0.236 *10*	C → 1309	5622.5 *6*	0.008 *2*	5623 → 0
4954.5 *7*	0.021 *3*	5939 → 984	5318.32 *25*	0.019 *3*	5319 → 0	5935.10 *11*	0.097 *10*	5936 → 0
4960.3 *4*	0.027 *3*	6018 → 1057	5360.93 *10*	0.119 *5*	6018 → 656	5938.1 *7*	0.011 *3*	5939 → 0
5033.50 *4*	0.620 *24*	6018 → 984	5543.67 *4*	0.410 *16*	C → 1057	6016.72 *6*	0.94 *4*	6018 → 0
5279.27 *10*	0.422 *20*	5936 → 656	5554.59 *11*	0.052 *4*	5555 → 0	6600.08 *8*	0.94 *4*	C → 0

[a]In our notation, 166.78 *5* ≡ 166.78 ± 0.05, etc.

[b]In our notation, 0.44 *4* ≡ 0.44 ± 0.04, etc. Multiply by 10.515 to obtain photons per 100 thermal neutron captures.

[c]See also Table IV. The symbol C denotes the capturing state.

[d]Deduced for one member of a close doublet from level energies obtained by an overall least-squares fit excluding this transition.

[e]Can also be placed as a 2044 → 1057 transition.

[f]Intensity balance at the 5936- and 1971-keV levels suggest that the peak observed at this energy corresponds mostly to the 5936 → 1971 transition. However, a small portion of this peak might represent a possible 3965 → 0 transition.

[g]Can also be placed as a 5283 → 656 transition.

F. Lifetime measurements

Also of importance in determining allowable J^π values are the electromagnetic transition strengths deduced from the level lifetimes. In Table VII we list previously reported lifetime results [25,27,41,51–57]. In many cases the lifetimes of ^{20}F states are either (i) unknown or (ii) known but with large uncertainties. In addition, there is reason to suspect that the lifetimes in the 10–100-fs range measured before 1983 are systematically too long [46]. Therefore, we have undertaken a detailed measurement of the level lifetimes.

Details concerning previous DSA measurements are given in Table VIII. Measurements made during 1969–1975, when the DSA method was still in its infancy, suffered from several shortcomings including (i) the use of the density value of bulk material without pausing to consider that the target was actually prepared by evaporation, (ii) the use of the Lindhard-Scharff-Schiøtt (LSS) theory [60], which has been shown through measurements to be inadequate, and (iii) the use of theoretically derived corrections [61] for large-angle scattering which introduce additional uncertainties in the analysis of data. In this work, significant improvements have been made by (i) using the entire line shape in the data analysis, (ii) making measurements with targets implanted in high stopping-power media, and (iii) simulating with the MC method the slowing-down process, experimental conditions, and the delayed feeding from higher-lying levels to the level being analyzed. Whereas in the past it was customary to arbitrarily increase the uncertainty in the extracted lifetime to reflect imperfect knowledge of the slowing-down mechanism, it has now become possible to extract these lifetimes much more reliably and accurately.

The current lifetime measurements were performed at the Accelerator Laboratory of University of Helsinki by application of the DSA method in conjunction with the reaction

TABLE III. Increasing complexity in the study of the ^{19}F$(n,\gamma)^{20}$F reaction.

Number of	Spilling *et al.* [28] Petten (1968)	Hardell and Hasselgren [29] Stockholm (1969)	Hungerford *et al.* [30] Grenoble (1983)	Kennett, Prestwich, and Tsai [31] McMaster (1987)	This work Los Alamos
γ rays	73	80	114	91[d]	168
spurious γ rays[a]	3	13	24	0	
placed γ rays[b]	66	73	90	91	165
primary γ rays	17	16	20	19	29
secondary γ rays	49	57	70	72	136
unplaced γ rays[c]	7	7	24	0	3
bound levels	23	19	25	25	36

[a]Gamma rays sought but not observed in this more sensitive work and, therefore, considered spurious.

[b]Some of the placed γ rays may be spurious.

[c]Some of the unplaced γ rays may be genuine.

[d]Only those γ rays that fit in the level scheme are listed by the authors.

TABLE IV. Level scheme of ^{20}F from the ^{19}F(thermal n, γ) reaction.

Compilation [9]		This work				
E (level)[a,b] (keV)	J^{π} [b]	E (level)[a] (keV)	Deexciting γ rays[c]	ΣI_{γ}(in)[a] (μb)	ΣI_{γ}(out)[a] (μb)	ΣI_{γ}(in−out)[a] (μb)
0.0	2^+	0.0		9471 *148*		9471 *148*
656.00 *4*	3^+	656.02 *3*	656.00	2067 *55*	1980 *100*	87 *114*
822.68 *8*	4^+	822.73 *3*	822.69, 166.78	617 *20*	659 *42*	–42 *46*
983.71 *5*	1^-	983.59 *3*	983.53	1189 *28*	1160 *60*	29 *66*
1056.82 *1*	1^+	1056.82 *3*	1056.78	1015 *47*	940 *40*	75 *62*
1309.34 *5*	2^-	1309.19 *3*	1309.17, 653.2, 325.73, 252.65	828 *26*	829 *30*	–1 *40*
1843.97 *8*	2^-	1843.80 *3*	1843.74, 1187.70, 534.60	638 *15*	668 *30*	–30 *34*
1970.80 *7*	(3^-)	1970.83 *4*	1970.73, 1148.05, 987.2, 661.63	486 *16*	509 *27*	–23 *31*
2044.05 *6*	2^+	2043.98 *3*	2043.89, 1387.90, 734.84	913 *24*	904 *30*	10 *39*
2194.36 *8*	(3^+)	2194.30 *3*	2194.16, 1371.53, 885.0	257 *11*	283 *11*	–26 *15*
2864.9 *15*	(3^-)	2864.86 *10*	2864.68, 2208.5, 2042.0, 1555.0, 1020.9, 894.1, 820.9, 670.1	44 *5*	42 *5*	2 *7*
2966.16 *8*	3^+	2966.11 *3*	2965.90, 2309.96, 2143.26, 771.71	336 *13*	336 *11*	0 *17*
3172.58 *42*	(1^+)	3171.69 *14*	2187.96	7 *2*	13 *2*	–6 *3*
3488.49 *6*	1^+	3488.41 *3*	3488.13, 2504.54, 2431.43, 2179.09, 1644.50	977 *32*	992 *43*	–15 *54*
3526.28 *7*	0^+	3526.31 *4*	2469.34	189 *8*	197 *8*	–8 *12*
3586.56 *9*	$(1,2)^+$	3586.54 *3*	3586.23, 2930.31, 2602.75, 2529.55, 1742.7, 1542.50, 1392.22, 620.44	818 *34*	882 *36*	–64 *49*
		3589.80 *4*	3589.47, 2933.76, 1545.87	211 *8*	214 *8*	–3 *11*
3680.13 *6*	1,2	3680.17 *4*	3679.91, 3023.90, 2623.18, 2370.88, 1836.50	199 *8*	187 *8*	12 *11*
3965.19 *16*	1^+	3965.07 *4*	2981.25, 2655.74, 2120.95, 793.36	123 *6*	134 *8*	–11 *10*
4082.08 *11*	$(1)^+$	4082.17 *4*	4081.77, 3098.1, 3025.10, 2038.08	156 *7*	152 *7*	4 *10*
4277.22 *14*	$(1,2)^+$	4277.09 *4*	3293.23, 3219.89, 2232.9	117 *5*	108 *6*	9 *8*
4371.38 *12*	(2^+)	4371.47 *11*	3387.56, 691.4	52 *5*	65 *5*	–13 *7*
4592.2 *29*		4591.72 *7*	3607.8, 3534.4	47 *4*	35 *4*	12 *6*
4891.6 *28*		4892.76 *17*	4070.0, 2697.9, 1306.2	26 *3*	20 *3*	6 *5*
5223.9 *23*	$(1,2)^-$	5226.1 *4*		5 *2*		5 *2*
5281.9 *25*		5282.79 *10*	5282.1, 4225.8	23 *2*	14 *3*	9 *4*
5318.87 *17*	0,1,2	5319.17 *4*	5318.32, 4335.09, 4262.5, 4009.3, 3475.3	86 *5*	84 *6*	2 *8*
5463 *3*	$(1,2,3)^+$	5465.89 *17*	2600.3	9 *2*	4 *2*	5 *3*
5555.34 *13*	1, 2^+	5555.34 *4*	5554.59, 4899.2, 4245.65, 3711.0, 2690.5	177 *9*	170 *7*	7 *12*
5620 *3*		5623.13 *6*	5622.5, 4639.0, 4313.29, 3578.6	61 *10*	58 *6*	3 *12*
5810.4 *25*	(1^+)	5810.1 *4*		4 *1*		4 *1*
5936.09 *5*	2^-	5936.13 *3*	5935.10, 5279.27, 4951.91, 4878.8, 4626.5, 4092.2, 3964.85, 3891.39, 3741.44, 3070.9, 2969.7, 2447.58, 2349.55, 2346.30, 2255.82, 1970.95, 1853.96	1490 *80*	1468 *31*	22 *86*
		5939.10 *10*	5938.1, 4954.5, 4095.01, 3894.2, 2352.44	102 *15*	89 *7*	13 *16*

TABLE IV. (*Continued*).

Complilation [9]		This work				
E (level)[a,b] (keV)	J^{π}[b]	E (level)[a] (keV)	Deexciting γ rays[c]	ΣI_{γ}(in)[a] (μb)	ΣI_{γ}(out)[a] (μb)	ΣI_{γ}(in−out)[a] (μb)
6017.77 *3*	2^-	6017.78 *3*	6016.72, 5360.93, 5033.50, 4960.3, 4708.19, 4173.54, 4046.71, 3973.47, 3823.05, 3152.1, 3051.43, 2529.20, 2431.08, 2427.83, 2337.58, 2052.8, 1935.50	3600 *150*	3614 *66*	−14 *164*
6044.98 *8*	0,1,2	6044.92 *3*	4735.22, 4200.56, 2556.35, 2458.0, 2079.72	202 *13*	195 *8*	7 *15*
6299 *4*		6299.1 *3*		5 *2*		5 *2*
	$0^+ + 1^+$	6601.35[d] *3*	6600.08, 5616.82, 5543.67, 5291.40, 4757.02, 4630.6, 4556.81, 3112.72, 3074.81, 3014.58, 2921.01, 2636.11, 2519.05, 2324.11, 2229.8, 2009.52, 1708.52, 1375.2, 1318.52, 1282.14, 1135.38, 1046.00, 978.19, 791.2, 665.21, 662.24, 583.55, 556.41, 302.2		9542 *180*	−9542 *180*

[a]In our notation, 656.00 *4* ≡ 656.00 ± 0.04, 9471 *148* ≡ 9471 ± 148, etc.
[b]For our independent evaluation of level energies and J^{π} values, see Table IX. In particular, our proposed J^{π} assignments for the levels at 2194, 3172, 3526, 3587, 3680, 3965, 4082, and 4277 keV differ from those listed in this column.
[c]See also Table II. The I_{γ} values listed there are in units of mb.
[d]Capturing state.

^{2}H(^{19}F, $p\gamma$)^{20}F. High recoil velocities (~4% of the velocity of light c) produced in this reaction guaranteed that the slowing down of the recoiling ^{20}F nuclei took place at velocities at which the electronic stopping power dominates and is experimentally known [62,63]. The level scheme of ^{20}F is sufficiently simple and the branchings from the excited states are sufficiently well known such that coincidence measurements were deemed unnecessary and reliable lifetimes could be extracted from the singles γ-ray spectra which were obtained, in most cases, with good statistics. Portions of γ-ray spectra from the current DSA measurements are shown in Fig. 3.

The 15-, 20-, and 28-MeV ^{19}F beams of about 200 particle nA were supplied by the 5-MV tandem accelerator EGP-10-II of the Accelerator Laboratory. The beams were focused to a 2×2 mm^2 spot on the target. The measurements were performed at three different bombarding energies in order to populate the desired levels and to vary the effect of the feeding transitions on the γ-ray line shapes.

The ^{2}H targets were prepared by implanting first 3.1×10^{16} at cm^{-2} 100-keV ^{20}Ne$^+$ and then 2.1×10^{17} at cm^{-2} 45-keV molecular $^2H_3^+$ ions into 0.8-mm-thick gold sheets. The ^{20}Ne implantation was necessary to provide trapping sites for ^{2}H and to avoid the diffusion of ^{2}H in Au [64]. The vacancies produced in the ^{2}H implantation migrated to the Ne-precipitate–Au interface and there effectively trapped the ^{2}H atoms [64,65]. A low stopping-power target was prepared by implanting 4.0×10^{18} at cm^{-2} 30-keV molecular $^2H_3^+$ ions into 0.4-mm-thick crystalline Si substrates.

The targets were contained in an air-cooled target holder made of stainless steel. The targets were set with their surfaces perpendicular to the beam direction. A vacuum better than 2 μPa was maintained in the target chamber to prevent carbon buildup on the target surface.

The γ rays were detected by an escape-suppressed spectrometer, which is described in Ref. [66]. The escape-suppression factor was ~4. The energy resolution of the spectrometer was 2.0 keV at E_{γ}= 1.33 MeV, 3.1 keV at 2.61 MeV, 3.9 keV at 3.33 MeV, and 5.4 keV at 6.29 MeV. The detector was located 55 mm from the target at 0° relative to the beam direction. A graded absorber (2.0 mm Pb, 1.0 mm Cd, and 1.5 mm Cu), set between target and the detector, reduced the counting rate due to low energy γ rays and x rays.

The γ-ray spectra were stored in a 16 384 channel memory with a dispersion of 0.537 keV/channel. For the line-shape analysis, the contents of adjacent channels were summed in cases where $E_{\gamma}>2.7$ MeV. The stability of the spectrometer was monitored with the 1461-keV ^{40}K laboratory background peak and with the stopped components of the γ-ray peaks from the decay of the long-lived 4967-keV state ($E_{\gamma}=3332.84\pm0.20$ keV, $\tau=4.8\pm0.5$ ps) in ^{20}Ne and the 6129-keV state ($E_{\gamma}=6128.629\pm0.040$ keV,

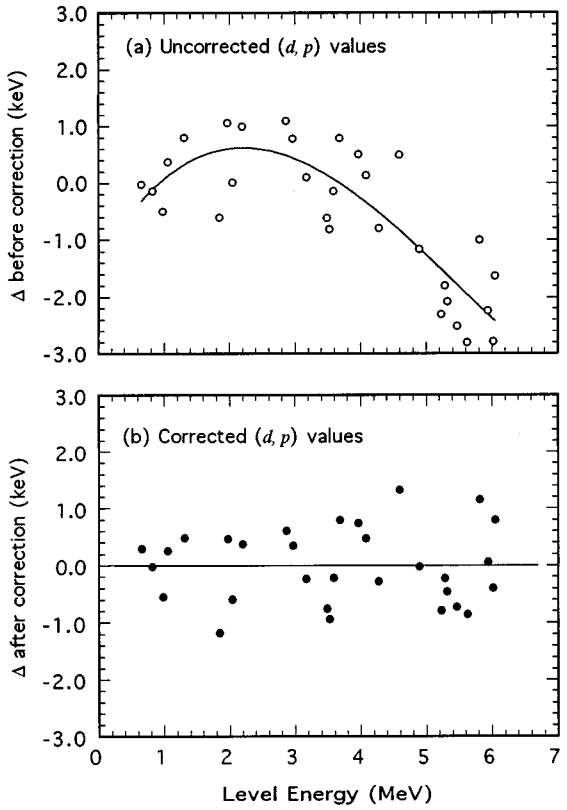

FIG. 2. Deviation Δ of the ^{20}F level energies measured in the (d,p) reaction [15] from the current (n,γ) values. Applying the correction given by the solid line (cubic polynomial) in (a) removes the systematic differences as shown in (b). The corrected values are given in Table V.

TABLE V. Energies of levels in ^{20}F obtained in the (d,p) reaction by Rollefson, Jones, and Shea [15] compared to those in the current (thermal n, γ) reaction. See also Sec. II B and Fig. 2. In our notation, 656.0 *11*≡656.0±1.1, 4311.5 *26*≡4311.5±2.6, etc. All energies are in keV.

(d,p)		(n,γ)[a]	(d,p)		(n,γ)[a]
Quoted	Corrected		Quoted	Corrected	
656.0 *11*	656.3	656.02	4311.5 *26*	4312.0	
822.6 *9*	822.7	822.73	4583.8 *30*	4584.6	
983.1 *8*	983.0	983.59	4592.2 *29*	4593.0	4591.72
1057.2 *9*	1057.1	1056.82	4730.2 *29*	4731.2	
1310.0 *8*	1309.7	1309.19	4763.8 *27*	4764.8	
1824.4 *16*	1823.8		4891.6 *28*	4892.7	4892.76
1843.2 *10*	1842.6	1843.80	4898.2 *28*	4899.4	
1971.9 *16*	1971.3	1970.83	5040.2 *31*	5041.5	
2044.0 *16*	2043.4	2043.98	5065.5 *31*	5066.8	
2195.3 *12*	2194.7	2194.30	5224.0 *31*	5225.5	5226.3
2866.0 *22*	2865.5	2864.86	5281.0 *33*	5282.6	5282.79
2966.9 *13*	2966.5	2966.11	5317.1 *27*	5318.7	5319.17
3171.8 *22*	3171.5	3171.69	5344.5 *33*	5346.1	
3487.8 *22*	3487.7	3488.41	5450.3 *38*	5452.1	
3525.5 *26*	3525.4	3526.31	5455.4 *32*	5457.2	
3586.4 *17*	3586.3	3586.54	5463.4 *33*	5465.2	5465.89
3681.0 *25*	3681.0	3680.17	5620.3 *33*	5622.2	5623.13
3760.9 *20*	3761.0		5762.8 *34*	5764.9	
3965.7 *19*	3965.9	3965.07	5809.1 *29*	5811.3	5810.1
4082.3 *19*	4082.6	4082.16	5933.9 *33*	5936.2	5936.13
4198.9 *27*	4199.3		6015.0 *38*	6017.4	6017.78
4207.7 *26*	4208.1		6043.3 *37*	6045.7	6044.92

[a]See Table IV.

$\tau = 26.6 \pm 0.7$ ps) in ^{16}O produced in the ^{2}H(^{19}F, n) and ^{2}H(^{19}F, $n\alpha$) reactions, respectively.

The DSA analysis was performed by computer simulation of the γ-ray line shapes with the MC method [67–73]. The measured dependence of the detector efficiency on the angle between the detector symmetry axis and the direction of γ-ray detection was taken into account in the line-shape simulations. Those calculational aspects that take into account the detector dimensions were verified with the fully shifted 6841-keV γ-ray peak in the data corresponding to the known short-lived ($\Gamma < 0.5$ keV, $\Gamma_\gamma = 0.34$ eV) $E_x = 11\,090$ keV state of ^{20}Ne [9] produced in the ^{2}H(^{19}F, n) reaction. A simulated line shape was a sum of the shapes corresponding to the direct and delayed feedings of a state. The sum was weighted by the experimental fractions of the feedings. The fractions of direct and delayed feedings were deduced from the measured intensities of the γ-ray transitions in ^{20}F and the γ-ray branching ratios of the states.

The kinematic broadening—defined as the ratio of the recoil velocity of the nucleus under study in the center-of-mass coordinate system to the velocity of the center of mass—determines the broadening of the fully Doppler-shifted γ-ray peak. At $E(^{19}\text{F}) = 20$ MeV, the broadening for different excited levels varied from 5.3% for the 5283-keV state to 13.8% for the 656-keV state, relative to the full amount of the shift. In the case of very short lifetimes ($\tau < 20$ fs), the observed shape of a γ-ray line depends also on (i) the angular distribution of emitted protons and (ii) the triple angular correlation between the beam direction, the direction of the emitted proton, and the angle of the γ-ray detection [74]. These two effects can be simulated by an ''effective'' center-of-mass angular distribution of proton emission, which was determined from the line shapes measured with the Si backing. In the case of longer lifetimes, the line shape is affected more by the slowing down than by the angular distribution or kinematic broadening.

Because the angular distributions and correlations for the ^{20}F levels were not explicitly known, an iterative procedure was used. An isotropic angular distribution used for the simulations of Au-backing data yielded the first approximation for the lifetime. This lifetime value was then used for the simulation of the angular distribution in Si-backing data. The angular distribution was adjusted until the χ^2 minimum was reached in the fitting of the γ-ray line shape. The obtained angular distribution was then used for the simulation in Au-backing data again. The iteration was continued until the convergence criteria were met; that is, until the changes in the effective angular distribution and in the mean lifetime value were negligible within the statistical uncertainties.

The stopping power of the slowing-down medium (Au or Si) for ^{20}F ions was described in the line-shape analysis according to the following equation:

TABLE VI. Branching ratios for levels in ^{20}F below MeV. See also Sec. II E. The J^π assignments are from Table IX.

E_i (keV)	J_i^π	E_f (keV)	J_f^π	Branching[a]	E_i (keV)	J_i^π	E_f (keV)	J_f^π	Branching[a]	E_i (keV)	J_i^π	E_f (keV)	J_f^π	Branching[a]
656	3^+	0	2^+	100	2194	3^+	0	2^+	43.5 *41*	3526	(0^+)	0	2^+	< 3
							656	3^+	< 1.1			984	1^-	< 2
823	4^+	0	2^+	33.4 *33*			823	4^+	47.4 *43*			1057	1^+	> 86
		656	3^+	66.6 *33*			1057	1^+	< 1.1			1309	2^-	< 3
							1309	2^-	1.7 *5*			1844	2^-	< 2
984	1^-	0	2^+	100			1824	5^+	< 1.1			2044	2^+	< 2
							1844	2^-	< 1.1			3172	(0^-)	< 2
1057	1^+	0	2^+	> 99.6			1971	(3^-)	< 1.4					
		656	3^+	< 0.4			2044	2^+	< 1.7	3587	(2)	0	2^+	33.3 *31*
												656	3^+	9.9 *13*
1309	2^-	0	2^+	91.6 *13*	2865	(3^-)	0	2^+	36 *13*			984	1^-	4.0 *7*
		656	3^+	2.4 *5*			656	3^+	5 *4*			1057	1^+	10.0 *35*
		984	1^-	4.9 *6*			823	4^+	13 *8*			1844	2^-	0.7 *4*
		1057	1^+	1.0 *3*			1309	2^-	12 *7*			2044	2^+	31.0 *30*
							1844	2^-	7 *5*			2194	3^+	8.8 *13*
1824	5^+	823	4^+	≥ 95			1971	(3^-)	7 *5*			2966	3^+	2.6 *4*
							2044	2^+	13 *8*					
1844	2^-	0	2^+	90.2 *16*			2194	3^+	7 *5*	3590	(3)	0	2^+	> 66
		656	3^+	6.6 *8*								656	3^+	> 7
		984	1^-	< 0.5	2966	3^+	0	2^+	27.1 *24*			823	4^+	< 7
		1057	1^+	< 0.7			656	3^+	12.3 *17*			1309	2^-	< 7
		1309	2^-	2.0 *5*			823	4^+	58.2 *30*			1971	(3^-)	< 3
							2194	3^+	2.4 *7*			2044	2^+	> 3
1971	(3^-)	0	2^+	17 *3*								2194	3^+	< 2
		656	3^+	< 1	2968	(4^-)	656	3^+	10 *10*			2865	(3^-)	< 3
		823	4^+	51 *5*			823	4^+	38 *10*			2966	3^+	< 2
		984	1^-	< 1			1309	2^-	12 *10*					
		1309	2^-	29 *5*			1971	(3^-)	40 *10*	3680	(2)	0	2^+	45 *5*
		1844	2^-	< 1								656	3^+	17 *4*
					3172	(0^-)	984	1^-	> 95			984	1^-	< 2
2044	2^+	0	2^+	7.3 *8*								1057	1^+	23 *4*
		656	3^+	90.1 *17*	3488	1^+	0	2^+	72.4 *42*			1309	2^-	5 *2*
		823	4^+	< 0.4			984	1^-	4.0 *6*			1844	2^-	8 *2*
		984	1^-	< 0.5			1057	1^+	7.1 *31*					
		1057	1^+	< 0.6			1309	2^-	9.2 *13*	3965	(1^+)	0	2^+	b
		1309	2^-	0.7 *2*			1844	2^-	7.4 *11*			984	1^-	25 *5*
		1844	2^-	< 0.4								1057	1^+	< 4
												1309	2^-	56 *6*
												1844	2^-	10 *3*
												3172	(0^-)	5 *2*

[a]In our notation, 33.4 *33* ≡ 33.4 ± 3.3, 43.5 *41* ≡ 43.5 ± 4.1, etc.

[b]See footnote f of Table II.

TABLE VII. Lifetimes of levels in ^{20}F obtained in the current and previous works.

	Previous work			This work: ^{2}H(^{19}F,$p\gamma$) reaction			
E_x(keV)	τ [a]	Method[b]	Ref.	E = 15 MeV τ [a]	E = 20 MeV τ [a]	E = 28 MeV τ [a]	Adopted τ [a]
656	357 $^{73}_{78}$ fs	Doppler shift attenuation	[41]	440 *30* fs			440 *30* fs
	370 *60* fs	Doppler shift attenuation	[52]				
	420 *50* fs	Doppler shift attenuation	[53]				
	390 *40* fs	Doppler shift attenuation	[55]				
	280 *90* fs	Doppler shift attenuation	[57]				
823	≥ 4.4 ps	Doppler shift attenuation	[41]		not measured		79 *6* ps
	76 *20* ps	Recoil distance[c]	[51]				
	0.9 $^{9}_{4}$ ps	Doppler shift attenuation	[52]				
	79 *6* ps	Recoil distance[d]	[27]				
984	1.28 $^{62}_{41}$ ps	Doppler shift attenuation	[41]	1.91 *12* ps	2.02 *12* ps		1.96 *9* ps
	1.8 *4* ps	Doppler shift attenuation	[52]				
	2.30 *25* ps	Doppler shift attenuation	[54]				
	1.8 *3* ps	Recoil distance[e]	[56]				
	0.95 $^{60}_{30}$ ps	Doppler shift attenuation	[57]				
1057	≤ 92 fs	Doppler shift attenuation	[41]	7.4 *21* fs	7.4 *22* fs		7.4 *16* fs
	45 *13* fs	Doppler shift attenuation	[52]				
	15 *6* fs	Doppler shift attenuation	[57]				
1309	1.11 $^{41}_{29}$ ps	Doppler shift attenuation	[41]	1.90 *11* ps	1.84 *12* ps		1.87 *9* ps
	0.8 *3* ps	Doppler shift attenuation	[52]				
	1.45 *25* ps	Doppler shift attenuation	[54]				
	1.9 *3* ps	Recoil distance[e]	[56]				
	> 1.6 ps	Doppler shift attenuation	[57]				
1824	≤ 65 fs	Doppler shift attenuation	[25]		not measured		≤ 65 fs
1844	30 *20* fs	Doppler shift attenuation	[52]	71 *5* fs	62 *5* fs		66 *5* fs
	26 *11* fs	Doppler shift attenuation	[57]				
1971	≥ 1.1 ps	Doppler shift attenuation	[25]	0.55 *12* ps	0.69 *13* ps		0.61 *9* ps
	1.40 *40* ps	Doppler shift attenuation	[54]				
2044	≤ 38 fs	Doppler shift attenuation	[41]	3.0 *9* fs	3.9 *9* fs	5.3 *11* fs	3.9 *7* fs
	37 *16* fs	Doppler shift attenuation	[52]				
	11 *6* fs	Doppler shift attenuation	[57]				
2194	≤ 46 fs	Doppler shift attenuation	[41]		4.3 *23* fs	4.0 *13* fs	4.1 *12* fs
	< 12 fs	Doppler shift attenuation	[52]				
	15 *6* fs	Doppler shift attenuation	[57]				
2865		not reported		25 *5* fs	33 *5* fs		29 *4* fs
2966	≤ 62 fs	Doppler shift attenuation	[41]	5.8 *19* fs	4.9 *21* fs	4.9 *16* fs	5.2 *11* fs
	60 *40* fs	Doppler shift attenuation	[52]				
	≤ 12 fs	Doppler shift attenuation	[57]				

TABLE VII. (*Continued*).

E_x(keV)	Previous work τ[a]	Method[b]	Ref.	This work ^{2}H(^{19}F,$p\gamma$) reaction E=15 MeV τ[a]	E=20 MeV τ[a]	E=28 MeV τ[a]	Adopted τ[a]
2968		not reported			not measured		
3172		not reported			not measured		
3488	< 47 fs	Doppler shift attenuation	[41]	11.5 *7* fs	12.3 *11* fs		11.7 *7* fs
	44 *11* fs	Doppler shift attenuation	[52]				
	20 *4* fs	Doppler shift attenuation	[57]				
3526	≤ 32 fs	Doppler shift attenuation	[41]	6.9 *10* fs	5.0 *9* fs	5.1 *7* fs	5.5 *6* fs
	30 *15* fs	Doppler shift attenuation	[52]				
3587	30 *30* fs	Doppler shift attenuation	[52]	0.9 *9* fs	1.6 *10* fs	1.0 *9* fs	1.1 *6* fs
3590		not reported			not measured		
3669		not reported			not measured		
3680		not reported		27 *3* fs	20 *5* fs	20.0 *21* fs	22.1 *23* fs
3761		not reported			not measured		
3965		not reported			6.9 *21* fs		6.9 *21* fs
4082		not reported		4.1 *11* fs	3.5 *12* fs	3.2 *11* fs	3.6 *7* fs
4199		not reported			not measured		
4208		not reported			not measured		
4277		not reported			11 *4* fs	4 *3* fs	7 *4* fs
4312		not reported		4.8 *8* fs	5.3 *11* fs	5.3 *10* fs	5.1 *6* fs
4371[f]		not reported				2.2 *17* fs	< 4 fs
5226		not reported			3.7 *15* fs	0.9 *7* fs	1.4 *11* fs
5283		not reported			2.6 *15* fs	4.4 *18* fs	3.3 *13* fs
5319		not reported				4.9 *11* fs	4.9 *11* fs
5555		not reported				6.0 *15* fs	6.0 *15* fs
5936		not reported				< 2 fs	< 2 fs
6018		not reported				3.3 *12* fs	3.3 *12* fs

[a] In our notation, $357\ ^{73}_{78} \equiv 357^{+73}_{-78}$, 440 *30* ≡ 440 ± 30, etc.
[b] For more experimental details concerning the Doppler-shift-attenuation measurements, see Table VIII.
[c] In the reaction ^{6}Li(^{18}O,$\alpha\gamma$).
[d] In the reaction ^{18}O(t,$n\gamma$).
[e] In the reaction ^{7}Li(^{18}O,$\alpha n\gamma$).
[f] Below this energy, all known levels are listed. Above, only those levels with measured lifetimes are listed.

TABLE VIII. Experimental conditions and analysis procedures used in the Doppler-shift-attenuation (DSA) lifetime measurements of ^{20}F levels. The measured values are based on the $F(\tau)$ analysis if not stated otherwise.

Reference	Reaction	v/c(%)	Slowing-down medium	DSA analysis
Current	^{2}H(^{19}F,$p\gamma$)	3.72–5.09	Au, Ge, and Si and implanted ^{20}Ne and ^{2}H	a
[53]	^{2}H(^{19}F,$p\gamma$)	4.77	200 μg/cm^2 Ti evaporated in deuterium atmosphere on Cu, Al, and Mg backings	b
[41]	^{19}F($d,p\gamma$)	0.70–0.95	250 μg/cm^2 CaF_2 evaporated on Cu backing	c
[52]	^{19}F($d,p\gamma$)	0.77–0.94	700 or 990 μg/cm^2 CaF_2 evaporated on thin C foils	d
[57]	^{19}F($d,p\gamma$)	0.79–1.13	75 μg/cm^2 CaF_2 evaporated on a 2.5 mg/cm^2 Au foil	e
[25]	^{18}O($t,n\gamma$)	0.65	40 μg/cm^2 $Ta_2{}^{18}O_5$ deposited on 10-μm thick Ta foil	f
[54]	^{3}H(^{18}O,$n\gamma$)	3.62, 3.97	260 μg/cm^2 tritiated Ti evaporated on Mg or Al	b
[55]	^{13}C(^{19}F,^{12}Cγ)	2.60, 2.75	20–30 μg/cm^2 enriched ^{13}C evaporated on 0.2-mm thick Ta or Ni sheets	g

[a]Doppler-broadened line-shape analysis (DBLA). Experimental stopping power. Computer simulation of the slowing-down process.

[b]DBLA. The nuclear stopping power was parametrized as $-(dE/dx)=K_n(v/v_0)^{-1}$ where $v_0 \approx c/137$. The parameter K_n was determined by fitting experimental projected range data or from Bohr's estimate [N. Bohr, K. Dan. Vidensk. Selsk. Mat. Fys. Medd. **18**, No. 8 (1948)]. The experimental electronic stopping-power data reported by D. I. Porat and K. Ramavataram [Proc. Roy. Soc. (London) **A252**, 394 (1959); Proc. Phys. Soc. (London). **A77**, 97 (1961); *ibid.* **A78**, 1135 (1961)] and by W. Booth and I. S. Grant [Nucl. Phys. **63**, 481 (1965)] were interpolated and fitted with $-(dE/dx)=K_e(v/v_0)-K_3(v/v_0)^3$, $v<v_c$; $-(dE/dx)=A+B(v/v_0)-C(v/v_0)^2$, $v\geq v_c$. The parameters K_3 and v_c were determined from the condition of continuity of (dE/dx) and its derivative at v_c. Nuclear and electronic stopping powers were included at velocities $v<v_c$. At velocities $v\geq v_c$, only the electronic stopping was used.

[c]Slowing down in target and backing were considered. An uncertainty of 20% in the electronic and nuclear stopping powers was included.

[d]Target tilted 45° with respect to the beam direction, to guarantee that no recoils escape the target before γ decay. An uncertainty of 20% in the electronic stopping power was included.

[e]Stopping power from the LSS theory [60] with the large-angle scattering corrections of Blaugrund [61].

[f]The electronic stopping parameter $K_e = 0.72$ keV cm^2/μg was used, based on extrapolation of the data of Porat and Ramavataram for Ne ions slowing down in gold.

[g]DBLA. Energy loss calculated according to $-(dE/dx)=K_n(v/v_0)^{-1}+K_e(v/v_0)-K_3(v/v_0)^3$. The parameters were deduced from experimental range data measured for 3- to 12-MeV ^{19}F ions in Ni and Ta.

$$\left(\frac{dE}{dx}\right)=\left(\frac{dE}{dx}\right)_e^{\text{expt}}+\left(\frac{dE}{dx}\right)_n^{\text{ZBL}}. \quad (1)$$

The values of the electronic stopping power $(dE/dx)_e$ of Au and Si for ^{20}F ions at velocities $v=(0.65–2.06)v_0$ (where $v_0 \approx c/137$ is the Bohr velocity, and c is the velocity of light) were interpolated from experimental values reported in Ref. [62] for ^{19}F. At velocities $v<0.65v_0$, the electronic stopping power was assumed to be proportional to v, with the slope based on the experimental value at $v=0.65v_0$. The experimental values reported in Ref. [63] for ^{19}F in Au were used at velocities $v=(2.5–12.7)v_0$, and the values at velocities $(2.06–2.50)v_0$ were interpolated from the values reported in Refs. [62] and [63]. The electronic stopping power of Si at ion velocities $v>2.06v_0$ was obtained from Ref. [75] and was scaled by a factor of 0.90 to match the experimental values at velocities $(0.0–2.06)v_0$ [62]. The uncertainty of the electronic stopping power was estimated to be ±5%.

The nuclear stopping power $(dE/dx)_n$ was calculated by the MC method, in which the scattering angles of the recoiling ions were directly derived from the classical scattering integral [67] and the interatomic interaction was described by the universal Ziegler-Biersack-Littmark (ZBL) potential [75]. In the cases studied here, the nuclear stopping power has only a small effect on the line shapes because recoil velocities are high and most of the states have short lifetimes.

The effect of the finite target thickness on the initial velocity of the recoiling ^{20}F nuclei was simulated in the DSA analysis by choosing the reaction depth randomly according to the ^{2}H depth distribution and by taking into account the energy loss of the ^{19}F beam at that depth. At a depth of 100 nm, typical values for the energy loss in Au were 600 keV at 15 MeV and 570 keV at 28 MeV. The corresponding values in Si were 195 and 155 keV, respectively. Depth distributions of ^{2}H in Si and Au were measured using the elastic recoil detection analysis (ERDA) technique [76]. Previous studies [67,68,77,78] on implanted targets indicate that the implanted layer has no significant effect on the density of materials probed by $v/c \approx 4\%$ ^{20}F recoils and, hence, on the extracted lifetimes.

In deducing the lifetime values in ^{20}F, we started with the highest-energy level that was populated significantly at a given bombarding energy and continued downward in exci-

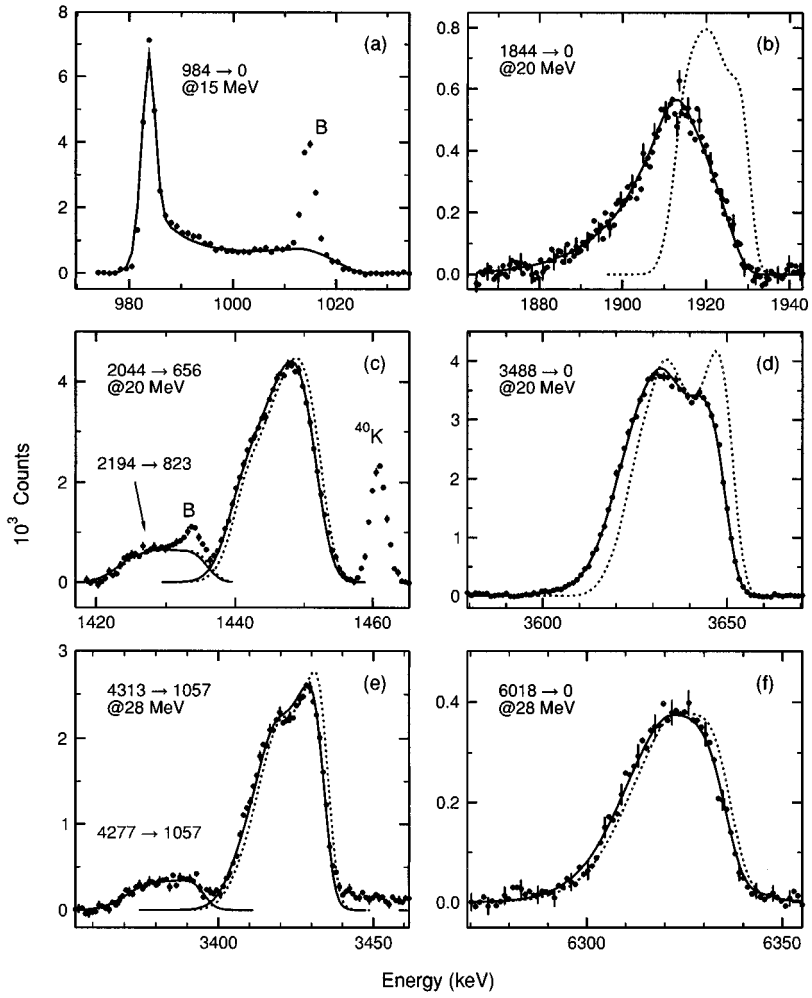

FIG. 3. Selected portions of background-corrected γ-ray spectra observed in the ^{2}H(^{19}F, $p\gamma$)^{20}F reaction on deuterium targets implanted in (a) silicon and (b)–(f) gold backings. See Sec. II F for related discussion. The bombarding energies are given in the figures. The simulated best-fit lineshapes corresponding to the lifetimes given in Table VII are shown by continuous lines. The dotted lines in (b)–(f) correspond to a lifetime of $\tau=0$ fs, and represent the effects related to reaction kinematics. The laboratory background peak arising from ^{40}K and background peaks *B* caused by the $(n,n'\gamma)$ reaction on surrounding material are marked in (a) and (c). The fast neutrons arise mainly from the ^{2}H(^{19}F, n) reaction.

tation energy. The branching ratios of the levels and the deduced lifetimes were entered as input data in the MC simulations of a line shape. Branching ratios and the probability of exciting a particular level were used to calculate the feeding fractions. Values used in this work are from (i) Table VI for all states below 4.0 MeV, (ii) current ^{2}H(^{19}F, $p\gamma$) experiment for the 4313- and 5226-keV states, (iii) Table II for those states above 4.0 MeV observed in the current (thermal n,γ) experiment, and (iv) Ref. [9] for all other states.

The level lifetimes measured in this work—several for the first time—are given in Table VII. As shown in that table, the current values are more accurate than previous ones. In addition, the current lifetimes for the levels at 1971, 2044, 2194, 2966, 3488, 3526, and 3587 keV are much shorter than those previously reported. When combined with the branching ratios given in Table VI, the lifetimes measured in this work yield absolute strengths for approximately 41 *E*1, 38 *M*1, and two *E*2 transitions in ^{20}F. The distributions of these strengths are consistent with the systematics for the $A=5$–20 region [79].

III. J^π ASSIGNMENTS FOR LEVELS IN ^{20}F

Because almost all the reactions that are likely to give useful information on the J^π values of levels in ^{20}F have already been studied—some several times—and because of the lessened activity in conventional nuclear spectroscopy expected in future years, significant new information on the J^π assignments of ^{20}F levels will likely appear with greatly reduced frequency. Thus, we think that a review of the currently available information (see Table IX) is timely. In what follows, no attention is given to chronological order. When more than one experiment is available for a given reaction, we list only the one that we think gives the more definitive result. When a definite assignment is made, only that information is usually given which is necessary to establish the J^π value.

Although not always mentioned, the ^{20}F(d,p) angular distributions and cross sections are probably the most important single input for these J^π assignments. For this reaction, we relied mainly on the work of Fortune and his collaborators [16,35–37]. Other relevant transfer reaction data are supplied by the ^{21}Ne($d,^3$He) [48] and ^{21}Ne(t,α) [49] proton-pickup angular distributions. The former appears to discriminate better between l_p values and thus is relied on more heavily. The two-nucleon transfer reaction ^{18}O(^{3}He,p) [17,18] provides less useful information than the one-nucleon transfers because of a lack of discrimination between L values, low cross sections (relative to the competing multistep processes), and poor predictive power for the theory (see, for example, Fig. 6 of Ref. [17]). However, γ-ray linear-polarization measurements [24] following the (^{3}He,p) reaction are crucial for establishing definite J^π assignments (especially $\pi=-$ assignments) for five of the

TABLE IX. Energy levels (E) in ^{20}F below 4.32 MeV and their spin and parity (J^π) assignments.

E(level) (keV)	J^π	Reasons for J^π assignments and remarks
0.0	2^+	J from angular correlation between β^- and circularly-polarized $2^+ \rightarrow 0^+$ γ rays in ^{20}Ne [45]. π from allowed nature ($\log ft = 4.99$) of the β^- decay to the first-excited 2^+ state of ^{20}Ne [44].
656.02 *3*	3^+	Strong $[(2J+1)S = 2.32]$ $\ell_n = 2$ in (d,p) [36] gives $J^\pi = 1^+, 2^+,$ or 3^+. Gamma-ray linear-polarization measurement [24] together with application of Eq. (2) and γ-ray correlation studies [22] chooses 3^+ over 1^+ or 2^+. $J^\pi = 1^+$ is ruled out also by $d_{5/2}$ transfer in $(\vec{d},p)$ [38].
822.73 *3*	4^+	From a linear polarization study [24] together with γ-ray correlation studies [22,27] and application of Eq. (2). See Appendix.
983.59 *3*	1^-	$J^\pi = 0^- - 3^-$ from the $\ell_p = 1$ assignment in $(d,^3\text{He})$ [48]. Linear polarization measurement on the $984 \rightarrow 0$ transition [24] in combination with γ-ray correlations [22] selects 1^-.
1056.82 *3*	1^+	Allowed nature ($\log ft = 3.74$) of the β^- decay from the ^{20}O ground state [46].
1309.19 *3*	2^-	$J^\pi = 0^- - 3^-$ from the $\ell_p = 1$ assignment in $(d,^3\text{He})$ [48]. Linear polarization measurement on the $1309 \rightarrow 0$ transition [43] in combination with γ-ray correlations [22] selects 2^-.
1823.8 *16*	5^+	For the 1824-keV level, linear polarization [24], γ-ray correlations [22,25], and Eq. (2) determine
1843.80 *3*	2^-	$J^\pi = 5^+$ or 3^+, with a strong preference for 5^+. Absence of $\ell_n = 2$ in (d,p) [36] or $L = 2$ in $(^3\text{He},p)$ [17] favors 5^+. Although no single measurement is definitive, the cumulative evidence is sufficient for a definite 5^+ assignment for the 1824-keV level. For the nearby 1844-keV level, $J^\pi = 0^- - 3^-$ from the $\ell_p = 1$ assignment in $(d,^3\text{He})$ [48]. Linear polarization [24] yields a definite 2^- assignment when combined with γ-ray correlations [22] and Eq. (2). The CNPR result for the 1824-1844 doublet is $\Sigma J = 6-8$ in $(^7\text{Li},p)$ and $\Sigma J = 7-11$ in $(^{11}\text{B},\alpha)$ [12,10].
1970.83 *4*	(3^-)	Applying Eq. (2) to the three certain γ branches from this level, we find that pure $E2$ radiation is allowed for the transitions to the ground state and the 823-keV level but not to the 1309-keV level, while pure $M2$ radiation is forbidden for all three. The $1971 \rightarrow 823$ and $1971 \rightarrow 1309$ branches restrict J^π to 2^+ or 3^-. Gamma-ray angular-correlation measurements [25] restrict J to 2 or 3 in support of the conclusion from the partial lifetimes; $J^\pi = 2^+$ is not favored because it calls for an unusually large $B(E2)$ value (47 ± 14 W.u.) for the $1971 \rightarrow 823$ transition. Low cross sections in one-nucleon transfer reactions [17,36] is most easily explained by a 3^- assignment.
2043.98 *3*	2^+	Strong $[(2J+1)S = 2.32]$ $\ell_n = 2$ in (d,p) [36] gives $J^\pi = 1^+, 2^+,$ or 3^+. From Eq. (2), the strong γ branch to the 656-keV, 3^+ level is predominantly dipole with $\lvert\delta(E2/M1)\rvert < 0.026$. When combined with angular correlation measurements [22], this information yields agreement with 2^+ and eliminates 1^+ and 3^+.
2194.30 *3*	3^+	Strong $[(2J+1)S = 0.55]$ $\ell_n = 2$ in (d,p) [36] gives $J^\pi = 1^+, 2^+,$ or 3^+. Gamma-branching and lifetime (Tables VI and VII) establish the $2194 \rightarrow 823$ transition as predominantly dipole.
2864.86 *10*	(3^-)	Low cross sections in one-nucleon transfer reactions [17,36] and γ-branching ratios (see Table VI) are most easily explained by a 3^- assignment.
2966.11 *3*	3^+	Closeness of these two levels complicates interpretation. It is clear from γ-decay studies that it is
2968.0 *15*	(4^-)	the 2966-keV state that has a sizable $\ell_n = 2$ cross section $[(2J+1)S = 0.38]$ in (d,p) [36] with essentially no contribution from the 2968-keV level; hence $J^\pi = 1^+, 2^+,$ or 3^+. When combined with the partial lifetime information by means of Eq. (2), this restriction leads to a definite 3^+ assignment for the 2966-keV level. With $J^\pi = 3^+$ and a reasonable $B(E2)$ value, a large χ^2 was obtained in Ref. [22] for the ground-state transition (this is also true for the level at 2194 keV). Because of the strong evidence for $J^\pi = 3^+$, we assume that this is an experimental difficulty. The 2968-keV level does not appear to be formed in any one-nucleon transfer reactions. The γ decay (see Table VI) suggests $J^\pi = 4^-$. The CNPR result for this doublet is $\Sigma J = 5-9$ in $(^7\text{Li},p)$ [12] and $(^{11}\text{B},\alpha)$ [10].

TABLE IX. (*Continued*).

E(level) (keV)	J^π	Reasons for J^π assignments and remarks
3171.69 *14*	(0^-)	Weakly populated in transfer reactions. Lifetime is unknown. Only reported γ-decay mode is to the 984-keV, 1^- level. Best CNPR estimate is $J=0-2$ from $(^7\text{Li},p)$ [12] and $(^{11}\text{B},\alpha)$ [10]. Because it is not fed from the capturing $0^+ + 1^+$ state or from the 5936- and 6018-keV, 2^- levels, this level has most probably $J^\pi = 0^-$ (See Sec. IV B). E(level) = 3175.6 ± 1.3 keV, reported in Ref. [42], differs significantly from our value.
3488.41 *3*	1^+	The 3488-keV level has $J^\pi = 1^+$ because the β^- decay from the ground state of ^{20}O is allowed ($\log ft = 3.65$) [46]. The 3526-keV level has $J^\pi = 0^+$ or 1^+ from $\ell_n = 0$ in (d,p) [35]. Lifetime and γ-decay data are consistent with either, but 0^+ is favored by both the weakness of excitation in (d,α) [16] and the absence of feeding from the 5936- and 6018-keV, 2^- levels in (thermal n,γ). The CNPR gives $\Sigma J = 0-2$ in $(^7\text{Li},p)$ and $\Sigma J = 0-1$ in $(^{11}\text{B},\alpha)$ [12,10].
3526.31 *4*	(0^+)	
3586.54 *3*	(2)	This doublet is unresolved in all particle reactions studied to date. It is very weakly excited in all transfer reactions and no reliable spectroscopic information is obtained thereby. The doublet is separated by the observation of γ rays. There is a strong primary γ-ray feeding the 3587-keV level in (thermal n,γ) and this fact, when combined with the γ-decay modes shown in Table VI, practically guarantees $J = 2$. The 3590-keV level is not directly fed by a primary γ ray but is fed fairly strongly by secondary transitions from the 5936- and 6018-keV, 2^- levels, thus suggesting $J = 3$. The various particle reactions add very little of a quantitative nature other than suggestions of $\Sigma J = 2-5$ in $(^7\text{Li},p)$ and $\Sigma J = 4-7$ in $(^{11}\text{B},\alpha)$ from the CNPR [12,10].
3589.80 *4*	(3)	
3669.0 *30*	(4^+)	Use of the CNPR, which suggests $\Sigma J = 3-6$ in the reactions $(^7\text{Li},p)$ [12], $(^{11}\text{B},\alpha)$ [10], and (d,α) [50], leads to this doublet. In these reactions, the 3669-keV level would be unresolved from the 3680-keV level, which most likely has $J = 2$. The 3669-keV level is not observed in (thermal n,γ) thus suggesting $J \geq 3$. An $L = 4$ pattern is observed in $(^3\text{He},p)$ [17] proceeding to this doublet. The combined results suggest $J^\pi = 4^+$ for the 3669-keV level and an essentially negligible cross section for the 3680-keV level in $(^3\text{He},p)$. Additional evidence for a 3669-keV level with rather high spin is the energies measured in the $(^7\text{Li},p)$ [12], $(^{11}\text{B},\alpha)$ [10], and $(^3\text{He},p)$ [17] reactions; 3674.2 ± 2.8, 3669 ± 5, and 3669.4 ± 4.9 keV, respectively. We assume that the latter represents the 3669-keV level alone and the first two weigh the 3669- and 3680-keV levels in the ratio 9:5. In that case, an excitation energy of 3669 ± 3 keV is obtained for this level. The 3680-keV level is formed too weakly in (d,p) and (t,α) to give reliable spectroscopic information. It is fed directly by a primary γ ray in (thermal n,γ) and also by secondary transitions from the 5936- and 6018-keV, 2^- levels. The γ-decay modes shown in Table VI—with decays to the 3^+ and 1^+ states—strongly favor $J = 2$ for this level.
3680.17 *4*	(2)	
3761.0 *20*	(≥ 3)	Formed very weakly in all transfer reactions. The CNPR gives $J = 1-3$ in $(^7\text{Li},p)$ and $J = 2-4$ in $(^{11}\text{B},\alpha)$ [12,10]. Decays mainly to the 656-keV, 3^+ level [25]. Lifetime is unknown. Not fed by primary or secondary transitions in (thermal n,γ); hence $J \geq 3$ is favored.
3965.07 *4*	(1^+)	Even though populated only weakly, the $L = 0+2$ angular distribution in $(^3\text{He},p)$ suggests a $J^\pi = 1^+$ assignment [18]. $J = 1$ is consistent with the current (thermal n,γ). See also Sec. IV A.
4082.17 *4*	(1^+)	Even though populated only weakly, the $\ell_n = 0+2$ angular distribution in (d,p) suggests a $J^\pi = 1^+$ assignment [36]. $J = 1$ is consistent with the current (thermal n,γ). See also Sec. IV A.
4199.3 *27*	≥ 3	Evidence for this doublet comes from a high-resolution (d,p) study [15]. Neither level is populated in the current (thermal n,γ), thus suggesting $J \geq 3$ for both levels. This conclusion is supported by the CNPR results of $\Sigma J = 8-13$ in $(^7\text{Li},p)$ [12] and $\Sigma J = 5-9$ in $(^{11}\text{B},\alpha)$ [10].
4208.1 *26*	≥ 3	
4277.09 *4*	$(1^+,2^+)$	$\Sigma J = 2-4$ in $(^7\text{Li},p)$ [12] and $\Sigma J = 0-2$ in $(^{11}\text{B},\alpha)$ [10]. The angular distribution $\ell_n = 2$ in (d,p) [35] and strong feeding from the capturing $0^+ + 1^+$ state lead to $J^\pi = 1^+$ or 2^+ for the 4277-keV level. The $\ell_n = 0$ in (d,p) [35] leads to $J^\pi = 0^+$ or 1^+ for the 4312-keV level, but the failure to observe this level in (thermal n,γ) favors a $J = 0$ assignment.
4312.0 *26*	(0^+)	

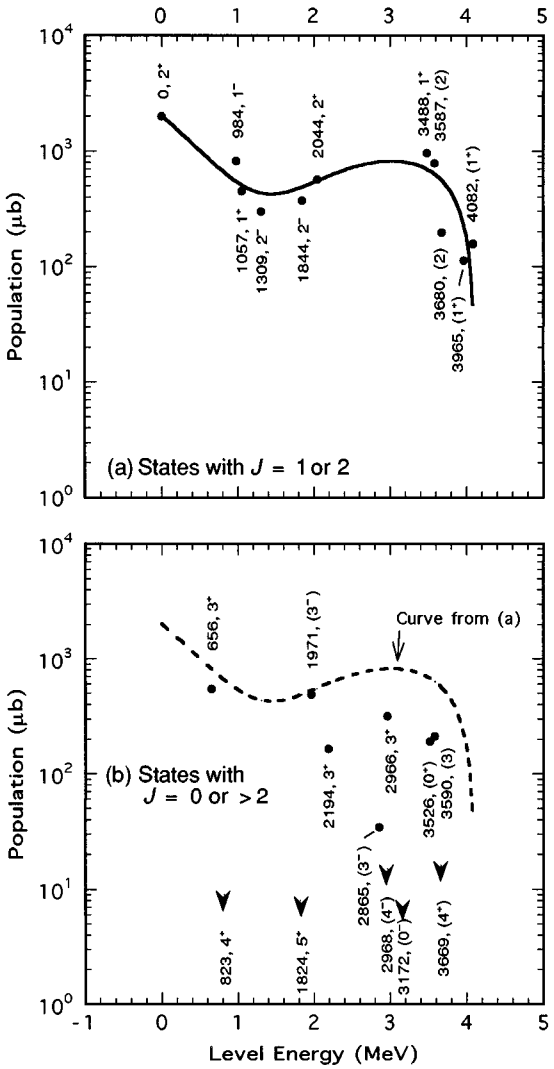

FIG. 4. Summed cross section for the population of low-lying states in ^{20}F (identified by their energy in keV and J^π value) from the neutron-capturing state, the 5936-keV level, and the 6018-keV level. See related discussion in Sec. III.

eight states in ^{20}F below 1.9 MeV.

The formation of states by primary γ transitions in the (thermal n,γ) reaction proceeds through two reaction mechanisms—direct and compound-nuclear capture. In both mechanisms, the primary transitions are almost exclusively dipole in nature. Thus, in the ^{19}F(thermal n,γ) reaction, with channel spins of 0^+ and 1^+ in the entrance channel, we expect formation of states with $J\leqslant 2$ by primary transitions and $J\leqslant 3$ by secondary transitions. In addition, this reaction is unusual in that $\sim$53% of all capture proceeds to two high-lying 2^- states at 5936 and 6018 keV. The deexcitation of these states, in turn, should lead to significant population of $J=1$–3 states. Therefore, if a particular low-lying state is populated strongly from all three states (the capturing $0^+ + 1^+$ state; the 5936-keV, 2^- state; and the 6018-keV, 2^- state), the spin of this low-lying state is most probably $J=1$ or $J=2$. The verification of this expectation is shown in Fig. 4(a). Conversely, if a particular low-lying state is either unobserved or observed with a relatively weak population in the (thermal n,γ) reaction, its spin is most probably $J\geqslant 3$ or (less likely) $J=0$. We have made use of this conclusion in assigning the J value for a few levels below 4.0 MeV. Our failure to observe any feeding to the known $J>3$ levels at 823 (4^+), 1824 (5^+), 2968 (4^-), and 3669 (4^+) keV is consistent with this conclusion [see Fig. 4(b)].

Another important determinant for J^π assignments is γ-ray angular-correlation studies in $A(b,c\gamma)$ reactions. We refer to the studies by Quin and Chagnon [20–23,39] and by Pronko [25,27] and their collaborators. The angular-correlation studies make use of limits set on J^π values and on quadrupole-dipole mixing ratios (δ^2) from consideration of limits on branching ratios and lifetimes. It is sometimes worthwhile to reconsider the angular-correlation results—all performed before 1974—in light of the more accurate branching ratios (see Table VI) and lifetimes (see Table VII) that are now available. In doing so, we form the partial lifetimes τ_p for various branches [by combining the level lifetime and γ branching ratios (and their uncertainties)] and then apply the recommended upper limits (RUL's) in Weisskopf units (W.u.) given by Endt [79]. For $A=20$, we have

$$B(E2)(\text{W.u.})=\frac{2.532\times 10^5\,\delta^2}{(E_\gamma)^5[\,\tau_p(0.1\%\text{C.L.})(1+\delta^2)}<100 \tag{2a}$$

and

$$B(M2)(\text{W.u.})=\frac{6.074\times 10^6\,\delta^2}{(E_\gamma)^5[\,\tau_p(0.1\%\text{C.L.})(1+\delta^2)}<5 \tag{2b}$$

with E_γ in keV and τ_p in s. In Eqs. (2a) and (2b), $\tau_p(0.1\%\text{C.L.})$ is the 0.1% confidence limit on the maximum partial lifetime formed by adding 3.3 times the standard deviation to τ_p. An example of the application of Eqs. (2a) and (2b) is given in the Appendix. In no case where the lifetime is known is a multipole higher than quadrupole of any significance, and we assume this is true for all states. We also assume that an appreciable part of the γ branching from a particular level proceeds by the lowest possible multipole order.

Fortune *et al.* [10,12–14] have studied the compound-nuclear reactions ^{14}N(^{7}Li,p), ^{16}O(^{7}Li,^{3}He), and ^{13}C(^{11}B,α) and have shown that the total cross sections for isolated levels in ^{20}F are—with some exceptions—closely proportional to $(2J+1)$. They exploit these reactions to make J estimates and to locate possible doublets that are unresolved in their experiment. For brevity, we will call this the compound-nuclear proportionality rule (CNPR). The ΣJ values for seven doublets (below 4.32 MeV) are given in Table IX and are used in making the J^π assignments for the individual members.

For most levels in ^{20}F, the J^π assignments have been made, both in Ref. [9] and in the current work, by combining the results from different experiments. Above 4.32 MeV, this procedure begins to break down because it becomes difficult to establish a one-to-one correspondence between the levels reported in different experiments. However, there are two levels at 5936 and 6018 keV for both of which a definite $J^\pi=2^-$ assignment can be made provided that we use the

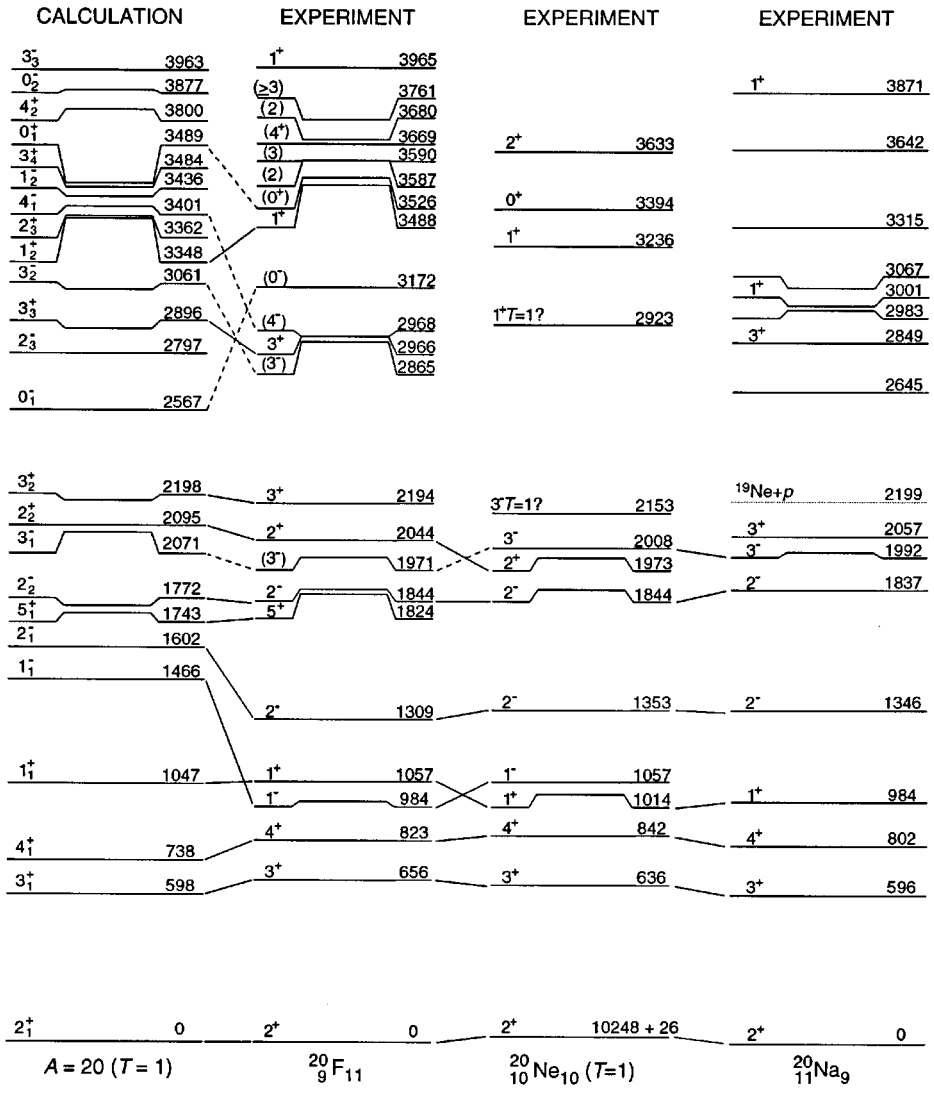

FIG. 5. Comparison between the WBN predictions of $T=1$ states below an excitation energy of 4.0 MeV and the experimental level schemes of ^{20}F, ^{20}Ne, and ^{20}Na. The levels are labeled by J^π on the left. The level energies shown on the right are in keV. The experimental level energies and J^π assigments for ^{20}F, ^{20}Ne, and ^{20}Na are from Table IX, Ref. [9], and Ref. [98], respectively. States are connected by solid lines if the correspondence between them seems certain and by dashed lines if speculative.

well-established correlation [2–8] between levels excited in the (d,p) and (thermal n,γ) reactions to establish such correspondences.

The (5936.09 ± 0.05)-keV level is fed by the 665.21-keV primary transition with a cross section of 1.49 ± 0.08 mb (see Tables IV and II), and the (6017.77 ± 0.03)-keV level by the 583.55-keV transition with a cross section of 3.60 ± 0.15 mb. These two transitions together account for $(53\pm2)\%$ of the total capture cross section of 9.51 ± 0.09 mb. It is also known from the (d,p) reaction that there are two strongly populated states whose energies are given as 5932 ± 5 and 6013 ± 5 keV by Rollefson and Aymar [34], and as 5941 ± 5 and 6026 ± 7 keV by Mosley and Fortune [37]. These two levels observed in (d,p) are most probably the same as the 5936- and 6018-keV levels observed in the (thermal n,γ) reaction. The 6018-keV level has an $l=1+3$ angular distribution in (d,p) [37], identifying it as a definite $J^\pi=2^-$ state. The 5936-keV level has an $l=1+(3)$ angular distribution, but because the $l=3$ component is uncertain, it is safer to identify it as a $J^\pi=1^-$ or 2^- state. However, a $J^\pi=1^-$ assignment can be ruled out because this level decays strongly to the 656-keV, 3^+ state (see the intensity for the 5279.27-keV transition in Table II). The 6018-keV level also decays strongly by means of the 5360.93-keV transition to the 656-keV, 3^+ state.

Note that we propose a new level at 5939.10 ± 0.10 keV very close to the level at 5936.09 ± 0.05 keV (see Table IV). These two levels would be unresolved in the (d,p) measurements of Ref. [37]; however, the population of the 5939.10-keV level by the 662.24-keV primary transition is only $\sim7\%$ of the population of the 5936.09-keV level by the 665.21-keV primary transition. Again using the correlation argument between the (thermal n,γ) and (d,p) reactions, it is reasonable to conclude that any contamination in the angular distribution of the 5936-keV level caused by the 5939-keV level would be small, leaving the $J^\pi=2^-$ assignment for the 5936-keV level intact.

IV. SHELL-MODEL CALCULATIONS

A. Levels in ^{20}F

Shell-model calculations for ^{20}F were performed with the recently constructed interactions of Warburton, Towner, and Brown [80,81] for the first four oscillator shells obtained from least-squares fits to two-body matrix elements (the WBT interaction) and to a potential (the WBP and WBN interactions). The $0p$ and the cross-shell $0p$-$1s$ $0d$ parts of these interactions are based on a least-squares fit of single-particle energies (SPE) and two-body matrix elements

TABLE X. Comparison of predicted and experimental observables for the ground state, the first two excited states, and the 1309-keV state in ^{20}F. In our notation, 2.094 *2*≡2.094±0.002, 0.043 *2*≡0.043±0.002, etc.

Initial state		Final state			Value	
J_n^π	E_x(keV)	J_n^π	E_x(keV)	Quantity	Prediction[a]	Experiment[b,c]
		2_1^+	0	μ(nm)	+2.508	+2.094 *2*
				Q(b)	+0.078	±0.043 *2*
3_1^+	656	2_1^+	0	$B(M1)$(W.u.)	0.191	0.25 *2*
				$B(E2)$(W.u.)	8.66	47 *47*
				$\delta(E2/M1)$	+0.050	+0.10 *5*
4_1^+	823	2_1^+	0	$B(E2)$(W.u.)	3.36	2.8 *4*
		3_1^+	656	$B(M1)$(W.u.)	0.053	0.058 *5*
				$B(E2)$(W.u.)	5.47	
				$\delta(E2/M1)$	+0.019	
2_1^-	1309	1_1^-	984	$B(M1)$(W.u.)	0.018	0.024 *3*
				$B(E2)$(W.u.)	4.87	
				$\delta(E2/M1)$	+0.060	

[a]Using the WBN interaction.

[b]The experimental values for the ground-state magnetic moment μ (in units of nuclear magnetons) and the quadrupole moment Q (in units of barns) are from P. Raghavan, At. Data Nucl. Data Tables **42**, 189 (1989). The Q value listed here supersedes the value given in Ref. [9]. The transition probabilities are in Weisskopf units (W.u.).

[c]When δ is not known, the $E2$ contribution of a mixed $M1+E2$ transition was assumed to be negligible (as predicted) in calculating $B(M1)$.

(TBME's) and/or a potential representation of them to 216 levels in the $A=10$–22 region assuming no mixing of $n\hbar\omega$ and $(n+2)\hbar\omega$ configurations. The $1s\ 0d$ TBME and SPE were taken to be those of Wildenthal's W interaction [82]. The $0p\ 1s\ 0d$ model space was expanded to include the influence of the $0s$ and $0f\ 1p$ shells by adding appropriate TBME's from other sources and by adjusting the SPE to reproduce selected experimental data [80]. The WBT, WBP, and WBN interactions are currently the most accurate available for describing level properties in the $A=10$–22 region.

The shell-model calculations were performed with the shell-model code OXBASH [83]. With this code, spurious center-of-mass motion is removed by the usual method [84] of adding a center-of-mass (c.m.) Hamiltonian $\mathscr{H}_{\text{c.m.}}$ to the interaction. Both even ($0\,\hbar\omega$) and odd ($1\,\hbar\omega$) parity spectra were calculated. The WBN spectrum is compared with experiment in Fig. 5. The even-parity spectrum of the WBN or WBT interaction is generated from the $(0p)^{12}(1s\ 0d)^4$ model space and is similar to that obtained with Wildenthal's W interaction [82]. A comparison of the WBT spectrum with experiment was made in Fig. 3 of Ref. [80]. The odd-parity spectrum is generated from the $0p^{-1}(1s\ 0d)^4 + (1s\ 0d)^3(0f\ 1p)^1$ configurations with the former dominant.

There is little uncertainty in the correspondence between experimental and theoretical levels up to 2.5 MeV in ^{20}F. This is so because the experimental J^π assignments are quite certain and the uncertainty in the theoretical energies is not large. It is pleasing that the gap between 2.2 and 2.8 MeV where no level is found experimentally is also reproduced (though less clearly) by the theoretical spectrum. Above 3.1 MeV there is more uncertainty in the correspondence between experimental and theoretical levels because (i) the J^π assignments of the experimental levels are ambiguous and there is the possibility of missing levels, (ii) the uncertainty in the theoretical energies increases significantly as the excitation energy increases, and (iii) ''intruder'' states, specifically $2\,\hbar\omega$ excitations of the $(0s)^4(0p)^{12}(1s\ 0d)^4$ type, are expected to appear in the 3–4-MeV region of excitation (see Sec. IV B). Apart from an unsuccessful attempt to identify definite experimental analogs to the calculated yrast states at $4.365(5_1^-)$, $4.458(7_1^+)$, and $4.524(6_1^+)$ MeV, no serious attempts were made, for the above reasons, to establish a one-to-one correspondence between experimental levels above 4.0 MeV and those from the shell model.

To aid in the identification of the $0\,\hbar\omega$ and $1\,\hbar\omega$ states of ^{20}F, an extensive calculation was made of the dipole and quadrupole transitions connecting the model states of Fig. 5. The $M1$ and $E2$ observables are expected to be predicted with considerable reliability [85]. The physics of $E1$ transitions is entirely different, and it is found that the $E1$ predictions are nearly worthless.

The general reason for the difficulty with $E1$ rates is the usual one. The $E1$ strength lies in the giant-dipole resonance (GDR), and the resulting reduction of strength in the transitions between the low-lying states is brought about by the mechanism of destructive interference between the allowable single-particle contributions. The nature of this destructive interference is of some interest. The $0p\leftrightarrow(1s,0d)$ transitions are intrinsically dominant. Yet, for the low-lying states, there

TABLE XI. Predicted $M1+E2$ and pure $E2$ branchings (with the WBN interaction) for excited states in ^{20}F with $E_x<3.53$ MeV compared with experimental values. The listed J^π values are our assumed correspondence with the shell-model predictions for $(0+1)\hbar\omega$ states (see Fig. 5). In our notation, 50 *6*≡50±6, 8.1 *7*≡8.1±0.7, etc. The entry "any other transition" refers only to $M1+E2$ and $E2$ branches.

Initial state		Final state			Relative branching		Initial state		Final state			Relative branching	
J_n^π	E_x(keV)	J_n^π	E_x(keV)	E_γ(keV)	WBN	Exp.	J_n^π	E_x(keV)	J_n^π	E_x(keV)	E_γ(keV)	WBN	Exp.
4_1^+	823	2_1^+	0	823	65.2	50 *6*	3_2^-	2865	1_1^-	984	1881	10.4	< 60
		3_1^+	656	167	100	100			2_1^-	1309	1556	100	100
									2_2^-	1844	1021	32.8	~58
1_1^+	1057	2_1^+	0	1057	100	100			3_1^-	1971	894	36.5	~58
		3_1^+	656	401	< 0.01	< 0.5							
							3_3^+	2966	2_1^+	0	2966	100	100
5_1^+	1824	3_1^+	656	1168	0.3	< 5			3_1^+	656	2310	26.8	45 *5*
		4_1^+	823	1001	100	100			4_1^+	823	2143	89.7	215 *15*
									1_1^+	1057	1909	< 0.01	< 4
2_2^-	1844	1_1^-	984	860	63	< 30			2_2^+	2044	922	1.2	< 4
		2_1^-	1309	535	100	100			3_2^+	2194	772	8.3	9 *1*
3_1^-	1971	1_1^-	984	987	0.9	< 4	4_1^-	2968	2_1^-	1309	1659	8.5	~30
		2_1^-	1309	662	100	100			2_2^-	1844	1124	0.3	
		2_2^-	1844	127	0.04	< 4			3_1^-	1971	997	100	100
2_2^+	2044	2_1^+	0	2044	6.3	8.1 *7*	0_1^-	3172	1_1^-	984	2188	100	100
		3_1^+	656	1388	100	100			any other transition			< 0.01	< 30
		4_1^+	823	1221	< 0.01	< 0.5							
		1_1^+	1057	987	0.05	< 0.7	1_2^+	3488	2_1^+	0	3488	100	100
									1_1^+	1057	2431	7.0	10 *4*
3_2^+	2194	2_1^+	0	2194	92	92 *7*			2_2^+	2044	1444	2.4	< 0.5
		3_1^+	656	1538	2.3	< 3			any other transition			< 0.01	< 0.5
		4_1^+	823	1371	100	100							
		any other transition			< 0.01	< 3	0_1^+	3526	2_1^+	0	3526	0.4	< 2
									1_1^+	1057	2469	100	100
									any other transition			< 0.01	< 2

is an almost complete cancellation between the various $0p\leftrightarrow(1s,0d)$ contributions. What is left then cancels strongly with the $(1s,0d)\leftrightarrow(0f,1p)$ contributions, which are relatively large in spite of the smallness of the $(0f,1p)$ terms in the wave functions because the $E1$ matrix elements are large compared to the $0p\leftrightarrow(1s,0d)$ matrix elements. The $(1s,0d)\leftrightarrow(0f,1p)$ contribution is not too well determined because the $(0f,1p)$ part of our interaction was not fixed by a least-squares fit—as was the $0p$ $1s$ $0d$ part—and because the $(0f,1p)$ orbitals are unbound in the $A\sim20$ region.

A further uncertainty in the calculated $E1$ rates arises from the large effect that $2\hbar\omega$ excitations of the even-parity states can have because they connect in first order to the $1\hbar\omega$ configuration. A $(0+2)\hbar\omega$ calculation of ^{20}F is beyond our current capabilities. Therefore, the possible role of $2\hbar\omega$ excitations in $E1$ transitions in this region was tested by a $1\hbar\omega\rightarrow(0+2)\hbar\omega$ calculation in ^{18}O. It was found that after the cancellations described above, the $1\hbar\omega\rightarrow2\hbar\omega$ contribution was comparable to the $1\hbar\omega\rightarrow0\hbar\omega$ contribution. A similar result should hold for ^{20}F. The difficulty with $E1$-like transitions was encountered previously [86] in calculations of the analogous first-forbidden β decays of $A=18$–20 nuclei and in the calculation of $E1$ transition rates in ^{17}N [87]. However, in the β-decay study, only rank-0 matrix elements were considered, and the rank-1 $E1$ matrix element has considerably greater problems because of the increased freedom in the allowable single-particle transitions; for example, the energetically favored $0\,d_{5/2}\leftrightarrow0\,f_{7/2}$ transition is allowed for rank 1 but not for rank 0.

The predicted $M2$ rates were all insignificant. Thus, we concentrate on $M1$ and $E2$ rates only. For the ground state, the first and second excited states, and the 1309-keV state, we make in Table X a detailed comparison between theory and experiment. The agreement is reasonable except possibly for the quadrupole moment of the ground state. For the remaining levels, we will concentrate on relative γ-branching ratios. In Table XI, the predicted $M1$ and $E2$ branching ratios for the states up to 3.53-MeV excitation are compared to experiment. We assume the J^π values corresponding to the association with model states made in Fig. 5. Although it is possible that the 3172-keV level is a 1^+ $2\hbar\omega$ state (see Sec. IV B), we assume here—for the sake of comparison—that it

TABLE XII. Comparison of predicted and experimental mean lifetimes τ of excited states in ^{20}F. The listed J^π values are our assumed correspondence with the shell-model predictions for $(0+1)\hbar\omega$ states (see Fig. 5). The experimental τ values are from the last column of Table VII. In our notation, 0.44 *3*≡0.44±0.03, 79 *6*≡79±6, etc.

States in ^{20}F		Predicted	Experiment
J_n^π	E_x(keV)	τ	τ
3_1^+	656	0.59 ps	0.44 *3* ps
4_1^+	823	79 ps	79 *6* ps
1_1^-	984	not calculated	1.96 *9* ps
1_1^+	1057	8.2 fs	7.4 *16* fs
2_1^-	1309	2.6 ps	1.87 *9* ps
5_1^+	1824	60 fs	≤ 65 fs
2_2^-	1844	28 fs	66 *5* fs
3_1^-	1971	0.18 ps	0.61 *9* ps
2_2^+	2044	5.3 fs	3.9 *7* fs
3_2^+	2194	3.7 fs	4.1 *12* fs
3_2^-	2865	22 fs	29 *4* fs
3_3^+	2966	3.4 fs	5.2 *11* fs
4_1^-	2968	98 fs	not known
0_1^-	3172	38 fs	not known
1_2^+	3488	9.2 fs	11.7 *7* fs
0_1^+	3526	4.5 fs	5.5 *6* fs

is the 0^- 1 $\hbar\omega$ state for which the experimental counterpart has been hitherto missing (see Fig. 5). With *E*1 transitions omitted from consideration, our method of comparison is to give relative *M*1 and *E*2 branchings for both experiment and theory. If desired, the experimental branching ratios for all decay modes (*E*1 included) can be calculated from the values of Table VI. Level lifetimes are estimated by multiplying the predicted partial *M*1 (*E*2) lifetime by the experimental *M*1 (*E*2) partial branching fraction. The predicted and experimental lifetimes are compared in Table XII.

The comparison of branching ratios given in Table XI shows good overall agreement. The discrepancies are all minor except that the 2966→823 keV transition is 2.4 times stronger than is predicted. The lifetimes are also in reasonable agreement (see Table XII). A serious discrepancy existed previously concerning the lifetime of the 1971-keV level. The reported values ($\tau \geqslant 1.1$ in Ref. [25] and $\tau = 1.4 \pm 0.4$ ps in Ref. [53]) were consistent but were much longer than the calculated value of 0.18 ps. The current value of 0.61 ± 0.09 ps decreases the discrepancy considerably.

There are five known energy levels between 3.55 and 3.80 MeV. These are close enough in excitation energy such that a comparison of experiment to the predicted branching ratios of a generic 3670-keV level can represent all five possible decays. The experimental branching ratios of the 3669- and 3761-keV levels are not known, although the 3761-keV level probably has a sizable branch to the 656-keV level [25].

TABLE XIII. Predicted $M1+E2$ and pure $E2$ branching ratios for a generic 3670-keV level with four different assumed J^π values for this level. The listed J^π values for the final states in ^{20}F are our assumed correspondence with the shell-model predictions for $(0+1)\hbar\omega$ states (see Fig. 5).

Final state		Branching ratios (%)			
J_n^π	E_x(keV)	2_3^+	3_4^+	4_2^+	2_3^-
2_1^+	0	59.4	90.4	0.1	
3_1^+	656	14.7	2.4	63.6	
4_1^+	823	0.01	3.2	16.2	
1_1^-	984				22.6
1_1^+	1057	6.4	0.0	0.0	
2_1^-	1309				52.6
5_1^+	1824		0.0	15.3	
2_2^-	1844				3.1
3_1^-	1971				20.6
2_2^+	2044	2.6	1.6	0.0	
3_2^+	2194	9.2	2.0	4.8	
3_2^-	2865				1.0
3_3^+	2966	7.7	0.4	0.0	
4_1^-	2968				0.0

From Fig. 5 it can be inferred that the theoretical 2_3^-, 2_3^+, 3_4^+, and 4_2^+ states are candidates for experimental levels in this energy range. In Table XIII, we show the predicted branching ratios for these four model states assumed to lie at 3670 keV. From a comparison of Tables VI and XIII, we make the following observations: (i) There is no good match of any of the predicted decays of Table XIII with the relevant decay modes of Table VI. (ii) A 2^+ assignment is suggested for the 3587-keV level because that choice most easily fulfills the need for the predicted 2_3^+ state. However, the comparison shows rather poor agreement for this choice—especially for the 3587→2044-keV branch—so we consider the identification as tentative. (iii) The 3590-, 3669-, and 3761-keV levels are possible candidates for the 3_4^+ state. The appreciable decays to the 1_1^+ state effectively remove the 3587- and 3680-keV levels from consideration. (iv) The predicted *M*1 and *E*2 decay modes of the 2_3^- model state do not fit at all well with the decays of the 3587- and 3680-keV levels to odd-parity states. (v) The signature of the 4_2^+ decay is a strong branch to the 5_1^+ state. None of the levels listed in Table VI has this feature. This leaves the 3669- and 3761-keV levels (with unknown or incompletely known branching information) as candidates for the 4_2^+ state.

An experimental counterpart to the 3436-keV, 1_2^- model state (see Fig. 5) has long been missing. Such a state should be populated appreciably in the current (thermal n,γ) measurement [see Fig. 4(a)]. Possible candidates are the levels at 3965 and 4082 keV (see Table IX), but at this time both levels have been preemptively assigned as positive-parity states by Medoff *et al.* [18] and by Fortune and Betts [36], respectively, and the $J^\pi = (1^+)$ assignments for both levels

TABLE XIV. Predicted and experimental spectroscopic strengths C^2S_p for proton pickup from ^{21}Ne leading to the states in ^{20}F below 3.0 MeV. The listed J^π values for the final states in ^{20}F are our assumed correspondence with the shell-model predictions for $(0+1)\hbar\omega$ states (see Fig. 5).

Final state			Spectroscopic strength		
J_n^π	E_x(keV)	ℓ_p	WBN	$(d,^3\mathrm{He})$	(t,α)
2_1^+	0	0+2	0.32+0.33	0.24+0.58	0.03+0.36
3_1^+	656	2	0.55	0.66	0.50
4_1^+	823	2	0.22	0.26	0.21
1_1^-	984	1	0.64	0.84	0.49
1_1^+	1057	0+2	0.32+0.33	0.08+0.25	0.02+0.12
2_1^-	1309	1	1.08	0.86	0.52
2_2^-	1844	1	0.06	0.69	0.28
3_1^-	1971	1	0.01		0.04
2_2^+	2044	0+2	0.32+0.33	0.01+0.15	0.01+0.13
3_2^+	2194	2	0.02	0.16	0.02
3_2^-	2865	1	0.06		0.09
3_3^+	2966	2	7.7		0.02

have become embedded in the literature. We consider the $\pi=+$ assignment for the 3965-keV level as particularly suspect because this level is excited only weakly in the ^{18}O(^{3}He,p) reaction and the comparison between the measured and empirical (^{3}He,p) angular distributions that has been used to assign $L=0+2$ is tentative at best.

We note that the comparison of branching ratios in Tables XIII and VI are of limited value at this time. Definite J^π assignments for levels above 2.8 MeV are needed before the correspondence between calculated and experimental levels can be firmly established and the ability of shell-model calculations to correctly reproduce the branching ratios can be fully tested.

Other experimental observables that can be compared to theory are the (d,p) stripping strength $(2J+1)S_n$, and the pickup strength C^2S_p, where C^2 is a Clebsch-Gordan factor equal to $\frac{2}{3}$ for the ^{21}Ne(d,^{3}He) and ^{21}Ne(t,α) pickup reactions that have been performed [48,49]. For the (d,p) stripping reaction, results for the *W* interaction (equivalent to the WBN reaction) are compared with experiment in Ref. [46]; the agreement is fair. Comparison of the WBN predictions to the results of the proton-pickup experiments is made in Table XIV. This comparison also shows fair agreement. The one large discrepancy concerns the 2_1^- and 2_2^- states for which experiment indicates considerably more sharing of the pickup strength than is predicted.

B. Level at 3172 keV

Below 4 MeV, a major difference between the current work and Ref. [9] concerns the J^π assignment for the 3172-keV level. Medoff *et al.* [18] have proposed 1^+ assignments for the (weakly populated) 3172- and 3965-keV levels on the basis of $L=0+2$ angular distributions in the ^{18}O(^{3}He,p) reaction, and these assignments have been adopted in Ref. [9]. In Ref. [18], the 1^+ assignment for the 3172-keV level is tentative because the $L=0$ component is small. Although not explicitly stated in Ref. [18], it is apparent from their figure that a mixture of $L=2$ and $L=0$ can easily mimic what actually might be an $L=1$ angular distribution.

The next 1^+ model state above that shown in Fig. 5 is predicted at 4748 keV. This energy is too high to permit associating this model state with the 3172- or 3965-keV level. Thus, if both of these levels have $J^\pi=1^+$, we believe they would be $2\hbar\omega$ states. We note that the γ-decay modes of the two levels are as one would expect for $2\hbar\omega$ states because neither level is known to decay strongly to $0\hbar\omega$ states.

As pointed out by Fortune *et al.* [36], the initial appearance of $2\hbar\omega$ intruder states at $\sim$ 3 MeV in ^{20}F, with a 1^+ state followed by a 1^+, 2^+, 3^+ triplet $\sim$ 1 MeV higher, is predicted by a weak-coupling estimate. In an attempt to make this estimate more quantitative, a $(0+2+4)\hbar\omega$ calculation was performed in a $0p_{1/2}\,0d_{5/2}\,1s_{1/2}$ model space with the Reehal-Wildenthal interaction [88]. The lowest predominantly $2\hbar\omega$ state was found to be a 1_3^+ state at 3.57 MeV. The calculation gives a fairly good account of the states (all predominantly $0\hbar\omega$) below this energy. The low-lying, predominantly $2\hbar\omega$ spectrum [J^π,E_x (in MeV)] is [1_3^+, 3.57], [2_4^+, 3.62], [3_4^+, 3.86], [3_5^+, 3.94], [4_3^+, 4.24], and [1_4^+, 4.38]. Because the predicted 1_3^+ energy is midway between that of the two candidates for the yrast $2\hbar\omega$ state—namely, the levels at 3172 and 3965 keV—the calculation offers no choice between the two. If the 3172-keV level is the lowest 1^+ intruder, we should expect a host of $2\hbar\omega$ states near or below 4 MeV. Thus, a definite J^π assignment for the 3172-keV level should be a high-priority goal.

The 1^+ assignment proposed for the 3172-keV level [18] has been recently questioned by Descouvement and Baye [89]. Using a microscopic cluster model, these authors calculate two $J=1$ states in the $\sim$ 3 MeV excitation energy region—a 1_2^+ state at 2.55 MeV and a 1_2^- state at 3.38 MeV. (These two states correspond to the 1_2^+ state at 3.348 MeV and the 1_2^- state at 3.436 MeV calculated in this work.) Both in Ref. [89] and in the current work, the former state is identified with the definitely known 1^+ state at 3.488 MeV. Through a process of elimination, Descouvement and Baye [89] propose that the 3172-keV level might correspond to the 1_2^- model state at 3.5 MeV.

We have difficulty reconciling the proposed 1^+ or 1^- assignment for the 3172-keV level [18,89] with the (thermal n,γ) data. The 3172-keV level is populated very weakly in the (thermal n,γ) reaction [$I_{793\gamma}$(in)$=7\pm2\,\mu$b and $I_{2188\gamma}$(out)$=13\pm2\,\mu$b]. In particular, we did not observe transitions (with $I_\gamma>3\,\mu$b) to this state from the capturing 0^++1^+ state; the 5936-keV, 2^- state; or the 6018-keV, 2^- state. It is possible that the special structure of the 3172-keV level (if it is, for example, a six-particle–two-hole 1^+ state as proposed in Ref. [18]) causes a specific transition to be very weak, but this explanation is unlikely to hold for all three transitions. Therefore, we prefer either a $J\geq3$ or a $J=0$ assignment for the 3172-keV level [see Fig. 4(b)]. The former can be excluded because the only known γ-decay mode of this level is to the 984-keV, 1^- state. If the $J=0$

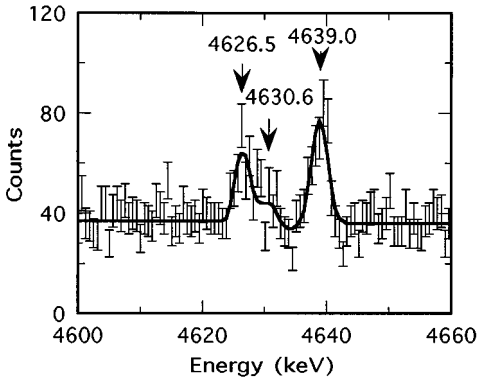

FIG. 6. Portion of the γ-ray spectrum from the $^{19}\mathrm{F}(n,\gamma)^{20}\mathrm{F}$ reaction with thermal neutrons showing resolution of the doublet at 4626.5 and 4630.6 keV. The 4630.6-keV γ ray might represent a primary $M2$ transition. See Sec. V A for related discussion.

assignment is correct, the parity cannot be positive because the angular distribution in $(^3\mathrm{He},p)$ [18] is either $L=2+(0)$ or $L=1$, but it is definitely not a pure $L=0$ as required by a 0^+ state. Therefore, we favor a $J^\pi=0^-$ assignment for the 3172-keV level. The negative-parity assignment is consistent with the absence of β^- feeding to this level ($I_\beta<0.012\%$, $\log ft>5.0$) in the β^- decay of ^{20}O [46]. In Fig. 5, we have associated this level with the 0_1^- shell-model state at 2567 keV.

Below 4 MeV, there is a one-to-one correspondence, with one notable exception, between the levels calculated using the cluster-model [89] and the shell model (this work). The exception is the 0_1^- state which is calculated in the former to lie at the much higher energy of 5.33 MeV compared to 2.567 MeV in this work. This overestimation is probably a result of choosing a cluster description of $^{16}\mathrm{O}+^3\mathrm{H}+n$ for describing the negative-parity states in ^{20}F instead of the more preferable, but computationally difficult, $^{15}\mathrm{N}+\alpha+n$ description. The overall agreement between the calculated and experimental level spectra (for both parities) is better with the shell model than with the cluster model. With both models, the agreement is much better, as expected, for the positive-parity states than for the negative-parity ones.

C. $T=1$ levels in ^{20}F, ^{20}Ne, and ^{20}Na

The expected mirror symmetry of the $T=1$ states in ^{20}F, ^{20}Ne, and ^{20}Na is shown in Fig. 5. This test is incomplete at this time because the level schemes of $^{20}\mathrm{Ne}\,(T=1)$ and ^{20}Na are not as well studied as that of ^{20}F. Nevertheless, it appears reasonably certain, just from this comparison, that the single levels in ^{20}Na at 984 and 1837 keV will eventually turn out to be 1^++1^- and 2^-+5^+ doublets, respectively. Similarly, the 2194-keV, 3^+ state in ^{20}F can be paired with the 2057-keV, 3^+ state in ^{20}Na, but the mirror partner of the 2044-keV, 2^+ state in ^{20}F is currently unknown in ^{20}Na.

The type of comparison shown in Fig. 5 is also important in nucleosynthesis, and this link has been discussed extensively in the literature (see, for example, Refs. [89–98] and references cited therein). The $^{19}\mathrm{Ne}(p,\gamma)^{20}\mathrm{Na}$ reaction is a leakage point from the hot CNO cycle, leading to a sequence of rapid proton (rp) capture and β decay that builds up elements extending to the iron-nickel region and beyond. The properties of ^{20}Na levels near the proton separation energy of 2199 keV, especially that of the first *known* unbound level at 2645 keV, governs the rate of this reaction. Because properties (spin, parity, and total width separated into proton and γ widths) of the 2645-keV level are uncertain, the method wanted has been to seek its mirror partner (in ^{20}F) and exploit the known properties of that partner.

The 2645-keV level is excited fairly strongly in the $^{20}\mathrm{Ne}(^3\mathrm{He},t)^{20}\mathrm{Na}$ reaction [47,91–93], and both Kubono *et al.* [91] and Lamm *et al.* [92] have proposed a $J^\pi=1^+$ assignment for this level on the basis of a comparison between the measured angular distribution and distorted-wave Born approximation (DWBA) calculations. They chose the 3172-keV level in ^{20}F, which had an erstwhile $J^\pi=(1^+)$ assignment (see Sec. IV B), as the mirror partner. However, the 2645-keV level is not fed in the β^+ decay of ^{20}Mg ($I_\beta<0.1\%$, $\log ft>6.2$ in the latest study [98]), thus suggesting either an incorrect J^π assignment or a complicated structure. The pairing of the 2645-keV level in ^{20}Na with the 3172-keV level in ^{20}F has been recently questioned—implicitly by Clarke *et al.* [47] and explicitly by Brown *et al.* [95]—by noting that in contrast to the strong excitation of the former level in the $^{20}\mathrm{Ne}(^3\mathrm{He},t)^{20}\mathrm{Na}$ reaction, the excitation of the latter level is very weak in the analogous $^{20}\mathrm{Ne}(t,^3\mathrm{He})^{20}\mathrm{F}$ reaction. These authors favor instead a $J^\pi=3^+$ assignment for the 2645-keV level in ^{20}Na on the basis of (i) similarity between the measured angular distribution for the triton group to this level with that for the ^{3}He group to the 2966-keV, 3^+ level in ^{20}F [47] and (ii) identification of the 2645-keV level and the 2966-keV level as mirror partners by a process of elimination and consideration of expected Coulomb shifts [95].

The estimated resonance strength is only 6 meV [92] if the 2645-keV level has $J^\pi=1^+$. It is an order of magnitude larger [95] if $J^\pi=3^+$. An attempt was made recently to study the $^{19}\mathrm{Ne}(p,\gamma)$ reaction using a radioactive ^{19}Ne beam and a polyethylene target [97]. An upper limit of 18 meV (90% confidence level) was deduced for the resonance strength, thereby favoring the $J^\pi=1^+$ choice (between $J^\pi=1^+$ and $J^\pi=3^+$) for the 2645-keV level.

Below 4.0 MeV, there are at least 22 excited states in ^{20}F (see Fig. 5). The lifetimes of 16 of these states are now known (see Table VII). This information should be of assistance in the spectroscopy of ^{20}Na because not only the level energies but also the transition rates should be similar for corresponding levels in these two nuclei.

V. SPECIFIC (n,γ) FEATURES

A. Possible primary $M2$ transition in ^{20}F

In the (n,γ) reaction, the observed γ rays originating from the capturing state (primary transitions) are predominantly $E1$ or $M1$. Of these two, primary $E1$ transitions are generally ($\sim$ 5–10 times) stronger than primary $M1$ transitions, but in the case of ^{20}F, because of the fullness of the $0p$ shell, primary $M1$ transitions (above 3.0 MeV) are, on the average, 2.5 times stronger than primary $E1$ transitions. The strongest primary transition from the 25-keV, 2^- neutron resonance [32,33] also appears to be $M1$ because it proceeds to the 1971-keV level, which has a tentative $J^\pi=3^-$ assignment (see Table IX).

Primary $E2$ transitions are extremely rare in the (n,γ) reaction [99–101]. In this work, primary $E2$ transitions to the known 3^+ levels at 656, 2194, and 2966 keV were not observed ($I_\gamma < 5\ \mu$b).

The only previously reported observation [102] of a primary $M2$ transition is in the ^{44}Ca(n,γ) reaction, but this result is erroneous [103]. As shown in Fig. 6, an extremely weak (~6 photons per 10^4 captures) 4630.6-keV γ ray was detected in the current ^{19}F(n,γ) work. The energy of this γ ray and the ultrapure nature of the ^{19}F target used in the experiment virtually guarantee that this γ ray does not originate from an impurity [104]. The most logical placement for this γ ray is between the capturing state ($J^\pi = 0^+ + 1^+$) and the 1971-keV, (3^-) level. If this placement and the 3^- assignment for the 1971-keV level are confirmed by future works, the 4630.6-keV γ ray would represent the first observation of a primary $M2$ transition in the (n,γ) reaction. (The 4630.6-keV γ ray can also be, in principle, an $M2 + E3$ transition, but any $E3$ component is expected to be negligible.)

B. Decays of the 5936- and 6018-keV levels

Several odd-parity bound levels in ^{20}F have both $E1$ primary transitions from the s-wave neutron-capturing state and p-wave spectroscopic factors determined from (d,p) measurements [36,37]. Most of these spectroscopic factors are small, as would be expected on the basis of constraints of the shell model, the $0p$ shell having been filled at ^{16}O and the $1p$ shell lying at a much higher excitation energy. Surprisingly, however, two high-lying 2^- states at 5936 and 6018 keV, bound by only 665 and 584 keV, respectively, have substantial spectroscopic factors that add up to ~ 28% of the total $1p$ strength. The primary transitions to these two levels are also very strong, and together account for ~ 53% of all captures. From each of these two states, we have observed 17 γ rays to the lower-lying states. To the best of our knowledge, the number of branches reported here (see Table XV) is the largest from any bound nuclear state.

Most of the secondary transitions from the 5936- and 6018-keV states are $E1$, and therefore, as we explained in Sec. IV A, are not well predicted by the shell-model calculations. The large number of γ rays from these states does allow us to use a statistical approach to judge if the similarity in their wave functions (as suggested by their large $1p$ components) leads to similar decay patterns. We therefore calculate the correlation coefficients for the transition strengths from the 5936- and 6018-keV states (denoted by subscripts 1 and 2 below) to the lower-lying states (denoted by f, running from the ground state 0 through a selected higher state n). This coefficient is defined as

$$\rho_n = \frac{\sum_{f=0}^{n} (T_{1f} - \langle T_1 \rangle)(T_{2f} - \langle T_2 \rangle)}{\sqrt{\sum_{f=0}^{n} (T_{1f} - \langle T_1 \rangle)^2 \sum_{f=0}^{n} (T_{2f} - \langle T_2 \rangle)^2}}, \qquad (3)$$

where T_{if} is a quantity related to the transition strength be-

TABLE XV. Decay patterns of the 5936-keV, 2^- and the 6018-keV, 2^- states to final states E_l in ^{20}F, and the linear correation coefficients ρ of paired reduced intensities [see Eq. (3)]. The correlation coefficients obtained when the $M1$ transitions to the levels at 984, 1309, 1844, 1971, and 2865 keV are enhanced by a factor of 5 are denoted by ρ^*.

E_f	$5936 \rightarrow E_f$		$6018 \rightarrow E_f$				
(keV)	E_γ(keV)[a]	I_γ(mb)[a]	E_γ(keV)[a]	I_γ(mb)[a]		ρ	ρ^*
0	5935.10 *11*	0.097 *10*	6016.72 *6*	0.94 *4*			
656	5279.27 *10*	0.422 *20*	5360.93 *10*	0.119 *5*	ρ_1	−1.0	−1.0
984	4951.91 *25*	0.059 *6*	5033.50 *4*	0.620 *24*	ρ_2	−0.996	+0.20
1057	4878.9 *6*	0.009 *2*	4960.3 *4*	0.027 *3*	ρ_3	−0.37	+0.42
1309	4626.5 *5*	0.008 *2*	4708.19 *12*	0.052 *4*	ρ_4	−0.18	+0.46
1844	4092.3 *4*	0.017 *3*	4173.54 *5*	0.167 *6*	ρ_5	−0.18	+0.46
1971	3964.85 *4*	0.441 *6*	4046.71 *23*	0.036 *3*	ρ_6	−0.35	−0.16
2044	3891.39 *25*	0.018 *3*	3973.47 *20*	0.024 *3*	ρ_7	−0.28	−0.11
2194	3741.44 *11*	0.058 *5*	3823.05 *9*	0.106 *6*	ρ_8	−0.28	−0.09
2865	3070.9 *3*	0.020 *3*	3152.1 *4*	0.014 *3*	ρ_9	−0.24	−0.08
2966	2969.7 *4*	0.016 *3*	3051.43 *4*	0.297 *12*	ρ_{10}	−0.22	−0.10
3488	2447.58 *4*	0.141 *7*	2529.20 *3*	0.58 *3*	ρ_{11}	+0.70	+0.05
3587	2349.55 *13*	0.031 *3*	2431.08 *3*	0.35 *3*	ρ_{12}	+0.63	+0.02
3590	2346.30 *16*	0.021 *4*	2427.83 *4*	0.190 *7*	ρ_{13}	+0.61	+0.01
3680	2255.82 *4*	0.087 *5*	2337.58 *14*	0.014 *3*	ρ_{14}	+0.47	−0.01
3965	1970.95 *5*	0.010 *3*	2052.8 *6*	0.005 *1*	ρ_{15}	+0.47	+0.01
4082	1853.96 *22*	0.013 *2*	1935.50 *5*	0.073 *5*	ρ_{16}	+0.47	+0.01

[a]From Table II.

tween states i and f, and $\langle T_i \rangle$ is the mean of these quantities for final states 0 to n. If we were to take the transition strength itself as the quantity T, we would expect to find a positive value of ρ_n as n moves to the higher-lying final states, even if the transitions are not actually correlated, because the E_γ^3 factor associated with dipole transitions causes the transitions from both the 5936- and 6018-keV states to a particular high-lying state to appear as weak, having the effect of a correlation according to Eq. (3). We therefore define T_{if} as the reduced transition strength—that is, the intensity of the gamma ray divided by E_γ^3.

With this definition of T, the values of ρ_n for the transitions from the 5936- and 6018-keV states are given in Table XV in the penultimate column. The pattern shows a marked break at ρ_{11}, thus indicating a swing toward positive correlation when the transitions to the higher-lying states are included. To test the significance of this swing, we have simulated sets of transitions in an uncorrelated model—the reduced transition strengths being drawn from a Porter-Thomas distribution, using sequences of pseudo random numbers. Histograms based on 10^4 trials are shown in Fig. 7 for ρ_3, ρ_{11}, and ρ_{16}. According to this figure, the chance of ρ_{11} being 0.70 or greater is only about 3% if all transitions to the states up to 3488 keV are uncorrelated. Similarly, the chance of ρ_{16} being 0.47 or greater is about 5%. The positive correlation might therefore be significant.

However, most of the high positive correlations from ρ_{11} upward appear to result from the pair of high intensities to the 3488-keV final state, coupled with generally weak intensities to the lower-lying states. The generally low averages resulting from the latter might be attributed to the considerable number of $M1$ transitions in this group. If we now try to make some allowance for the expected weakness of $M1$ transitions compared with $E1$ transitions, we obtain a quite different pattern of correlation coefficients from the experimental data. For example, if we enhance the $M1$ transitions by a factor of 5 (an approximate factor generally found in studies of primary transitions from neutron resonances), we obtain the final column (labelled ρ^*) of Table XV. The values listed there indicate no evidence at all for a correlation in the γ-ray branching from the 5936- and 6018-keV states. This result suggests that despite their closeness in energy, these two 2^- states do not show significant mixing.

C. Completeness

A large number of measurements (see Table I) has contributed information on approximately 88 bound levels in ^{20}F below the neutron separation energy of 6.601 MeV. The current shell-model calculation predicts correctly the total observed level density up to 4.6 MeV (see Fig. 8). The underprediction above this energy is probably caused by states arising from core excitations that are omitted in this and previous shell-model calculations [105].

The sensitivity of the current ^{19}F(thermal n,γ) measurements is such that a majority of levels with $J \leqslant 3$ should be observable in this work. However, because of the E_γ^3 factor associated with dipole transitions, we do not expect to see many levels above 6.1 MeV. The level scheme presented in Table IV consists of 35 levels below this energy. The shell-model calculations yield the following distribution of states:

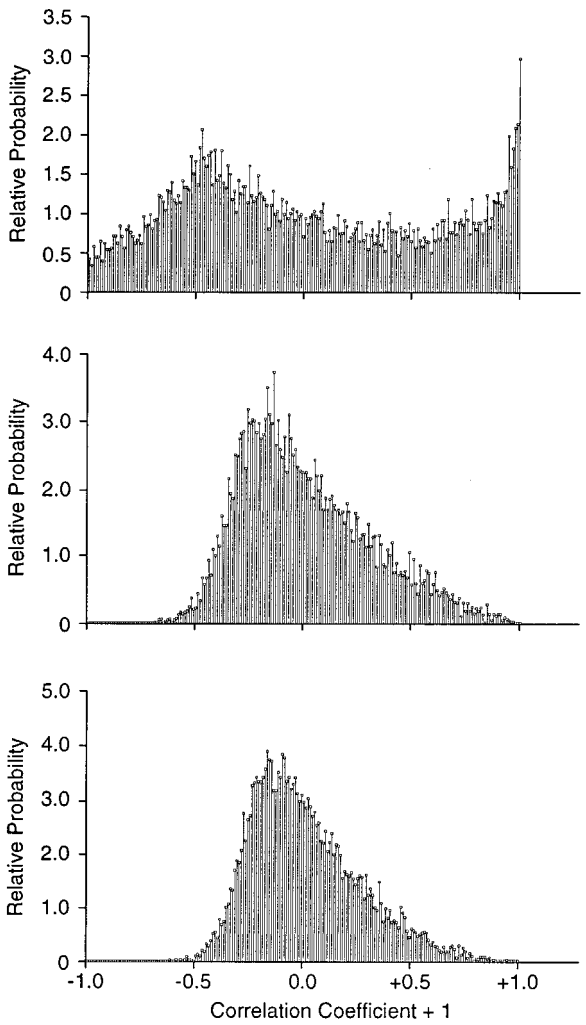

FIG. 7. Correlation coefficients [see Eq. (3)] simulated by the Monte Carlo method with 10^4 trials from assumed Porter-Thomas distribution of transition strengths to various numbers of final states. The relative probability scale is the probability of the correlation coefficient falling into the appropriate bin, divided by half the bin width. In this figure, the bin width is 0.01. (a) Four final states ($n=3$), (b) 12 final states ($n=11$), and (c) 17 final states ($n=16$).

$1\,(0^+)$, $2\,(0^-)$, $5\,(1^+)$, $5\,(1^-)$, $6\,(2^+)$, $7\,(2^-)$, $5\,(3^+)$, and $6\,(3^-)$ for a total number of 37 states with $J \leqslant 3$ below 6.1 MeV. This comparison suggests that the (n,γ) level scheme is reasonably complete.

VI. COMPARISON OF CAPTURE DATA WITH CALCULATIONS

A. Other relevant data

The total thermal-neutron-capture cross section of ^{19}F is small, already indicating a weakness of admixture in the initial (target + s-wave neutron) wave function from nearby resonances [positive (real) or bound (virtual)]. The total scattering cross section, $\sigma_{nn,\mathrm{tot}} = 3.64 \pm 0.01$ b, [59] on the other hand, is rather high for a light nucleus. The incoherent scattering cross section is very small, $\sigma_{nn,\mathrm{incoh}} = 0.40 \pm 0.02$ b, [59] implying that the potential scattering lengths of the two spin states formed in the slow-neutron reaction with ^{19}F (tar-

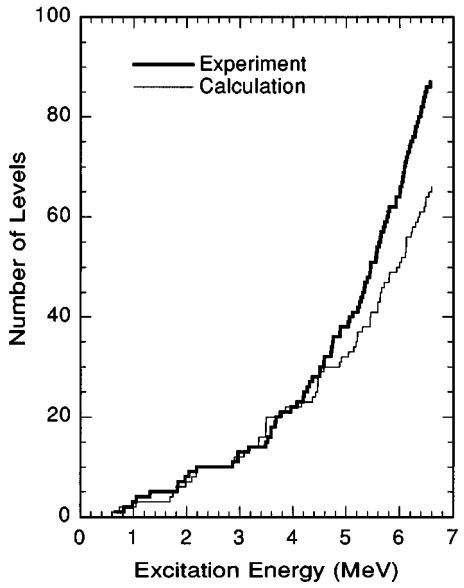

FIG. 8. Running sum of experimental levels and shell-model states in ^{20}F below the neutron separation energy of 6.601 MeV. The latter were calculated with the interaction and model space described in Sec. IV A.

get spin $J=1/2$) are nearly equal. In fact, the scattering lengths deduced from measurements are $a_{J=0}=5.48\pm0.02$ fm and $a_{J=1}=5.35\pm0.02$ fm. These values are to be compared with the potential radius, $R=3.70$ fm, expected from the optical model, and with the potential scattering length $a_{\rm pot}\approx4.6$ fm using the optical-model parametrization of Moldauer [106]. The summed ratios of reduced neutron width to energy of the local levels, $\mathscr{R}_{\rm loc}$, account for the difference between the observed scattering lengths and the potential scattering length through the relation

$$a_J=a_{\rm pot}-R\mathscr{R}_{J,\rm loc}. \tag{4}$$

The significantly higher values of the measured scattering lengths indicate some influence from local bound levels despite the evidence otherwise from the capture cross section. The two indications can be reconciled by assuming that such local levels are rather strongly bound. This hypothesis is supported by the resonance data. The lowest *s*-wave resonance is found [59] at the neutron energy of 269 keV, and no other confirmed *s*-wave resonances appear to have been located. Hence, the level spacing is large—on the order of, or greater than, a few hundred keV.

For the theoretical analysis of capture data we require, besides the free nuclear scattering lengths (discussed in the preceding paragraph), the final-state (d,p) spectroscopic strengths which were obtained from Refs. [36,37].

B. Capture cross sections of ^{19}F

In a series of papers [2–4], we have developed reliable methods for calculating slow-neutron-capture cross sections resulting from the direct-capture mechanism. In the first method, a specialized optical model $[S]$ is found for the nucleus under consideration, and its parameters are used to calculate the direct-capture cross section numerically. In the second method that we developed in Ref. [4], the potential-capture cross section $\sigma_{{\rm pot},\gamma}$ and the strength function for valence radiative transitions, $s_{\lambda,\rm val}$, from local levels are computed from the global optical model, together with the potential scattering length $a_{\rm pot}$ and the neutron strength function $\overline{\Gamma_n^0}/D$. The difference between the observed and the potential scattering lengths gives a measure of the contribution of local levels to the initial-state wave function [see Eq. (4)], and, hence, in conjunction with $s_{\lambda,\rm val}$, to the radiative transition amplitude. We denoted this method by $[G+V]$ in previous papers. The results from this method have always been found to agree closely with those of the $[S]$ method (when physically reasonable optical-model parameters can be found in the latter approach), and we now use the $[G+V]$ method almost exclusively.

The parameters of the global optical model used in our calculations are essentially those of Moldauer [106]. For the real potential, we use a Woods-Saxon form with a depth parameter $\mathscr{V}_0=-46$ MeV, surface diffuseness parameter $d=0.62$ fm, and potential radius $R=(1.16A^{1/3}+0.6)$ fm. The imaginary component of the potential has Gaussian form centered around the potential radius, with peak magnitude $\mathscr{Z}_0=-15$ MeV and width parameter $b=0.7$ fm.

In Table XVI, we give the calculated direct-capture cross sections for primary $E1$ transitions using the $[G+V]$ method together with data on the measured cross sections, the final-state spins (where known), and the spectroscopic strengths. In the final column, we list the rough estimates of cross sections resulting from the compound-nuclear mechanism, based on the assumption that this mechanism accounts for the discrepancies between the observed cross sections and the calculated direct-capture values. If the experimental uncertainty in the measured cross section $\sigma_{n\gamma}$ is ignored and if we assume that just one of the two initial spin states contributes the major part of the direct-capture cross section, random addition of the amplitudes of direct capture and compound-nuclear capture gives the approximate relation

$$\sigma_{\gamma({\rm CN})}\approx[\sigma_{n\gamma}^{1/2}\mp\sigma_{\gamma({\rm dir})}^{1/2}]^2. \tag{5}$$

In most of our previous studies of thermal-neutron capture by light nuclei [1–8], we found that direct capture dominates the cross sections, allowing the extraction of the compound-nuclear component [using Eq. (5)] as if it were a small perturbation; that is, we took the smaller of the two possible values of $\sigma_{\gamma({\rm CN})}$ in assessing its overall contribution. In this study, the direct-capture cross section is found to be very small because of the filled status of the $0p$ shell and the high-lying nature of the $1p$ single-particle strength. Hence, even a small compound-nuclear component may be similar in magnitude to the direct component. We thus have to consider both values of $\sigma_{\gamma({\rm CN})}$ given by Eq. (5).

To discuss the hypothesized compound-nuclear cross sections, we first divide out the normal $E1$ γ-ray energy dependence E_γ^3 to give ''reduced'' compound-nuclear cross sections. If we first use only the small values that result from Eq. (5), we find the mean value of $\sigma_{\gamma({\rm CN})}/E_\gamma^3$ for all 13 primary $E1$ transitions listed in Table XVI to be 210×10^{-6} b MeV^{-3}. Much the largest individual value is that for the transition to the 6018-keV state, which, at nine times the average, is at the $\sim0.25\%$ confidence level. (The confidence level is defined as the probability of finding a

TABLE XVI. Direct-capture cross sections for primary $E1$ transitions in the $^{19}F(n,\gamma)^{20}F$ reaction. Columns 1, 2, and 3 give the energy, J^π value, and the (d,p) spectroscopic factor S multiplied by $(2J+1)$ for the final state. Column 4 is the primary transition energy. Columns 5 and 6 give the average valency-capture width and the potential-capture cross section, respectively, both calculated using a global optical potential [see Eqs. (4)–(7) in the first listed reference of Ref. [4]]. The entries in column 5 do not include the spin-coupling factor and the spectroscopic factor; those in column 6 do. Column 7 is the calculated cross section using the global plus valence $[G+V]$ procedure. The experimentally determined cross sections are given in column 8. Finally, column 9 gives the minimum hypothesized compound-nuclear contributions deduced from the differences between column 7 and column 8 [see Eq. (5)]. In the table subheading, $a(X)$ refers to the experimental scattering length, while $a(G)$ and $\overline{\Gamma_n^0}/D$ refer to the scattering length and the neutron strength function, respectively, both calculated using the global optical potential.

E_f (keV)	J^π	(d,p) $(2J+1)S$ [a]	E_γ (keV)	$\Gamma_{\gamma,\mathrm{val}}/DE_\gamma^3$ $(10^{-7}\,\mathrm{MeV}^{-3})$	$\sigma_{\mathrm{pot},\gamma}$ (mb)	$\sigma_\gamma[G+V]$ (mb)	$\sigma_\gamma[X]$ (mb)	$\sigma_{\gamma(\mathrm{CN})}$ (mb)
$^{19}F(n,\gamma)^{20}F$ reaction; $a(X)_{J=0}=5.48$ fm; $a(X)_{J=1}=5.35$ fm; $a(G)=4.60$ fm; $\overline{\Gamma_n^0}/D=5.14\times10^{-4}$								
984	1^-	0.014 $(0p_{1/2})$	5617	0.387	0.171	0.055	0.138 *6*	0.019
1309	2^-	0.017 $(0p_{3/2})$	5291	0.506	0.276	0.109	0.236 *10*	0.024
1844	2^-	0.020 $(0p_{3/2})$	4757	0.570	0.220	0.096	0.189 *8*	0.016
4372	if 1^-	0.003 $(1p_{3/2})$	2230	1.023	0.025	0.015	0.052 *5*	0.011
	if 2^-					0.016		0.010
4592	if 1^-	0.02[b] $(1p_{3/2})$	2010	1.145	0.155	0.096	0.047 *4*	0.009
	if 2^-					0.102		0.010
5046	if 1^-	0.026 $(1p_{3/2})$	1555	1.502	0.168	0.113	< 0.006	~ 0.1
	if 2^-					0.118		~ 0.1
5226	if 1^-	0.09 $(1p_{3/2})$	1375	1.706	0.532	0.369	0.005 *2*	0.29
	if 2^-					0.385		0.30
5319	if 1^-	0.033 $(1p_{3/2})$	1282	1.833	0.185	0.130	0.086 *5*	0.005
	if 2^-					0.136		0.006
5466	if 1^-	< 0.07 $(1p_{3/2})$	1135	2.074	0.357	< 0.258	0.009 *2*	< 0.17
	if 2^-					< 0.268		< 0.18
5555	if 1^-	0.03 $(1p_{3/2})$	1046	2.252	0.143	0.105	0.177 *9*	0.009
	if 2^-					0.109		0.008
5810[c]	if 2^-	0.10 $(1p_{3/2})$	791	2.977	0.378	0.301	0.004 *1*	0.24
5936	2^-	0.43 $(1p_{3/2})$	665	3.533	1.40	1.14	1.49 *8*	0.023
6018	2^-	0.68 $(1p_{3/2})$	584	4.014	1.98	1.64	3.60 *15*	0.38

[a] From Refs. [36] and [37].

[b] This value, deduced for a peak at 4587 keV in Ref. [37], was assigned to a level at 4584 keV in Ref. [9]. It is assigned to the 4592-keV level in this work.

[c] The (d,p) angular distribution [37] leading to this state is consistent with either $\ell=1+3$ (suggesting $J^\pi=2^-$) or $0+2$ (1^+).

specific value of reduced compound-nuclear cross section, or greater, assuming the Porter-Thomas distribution.) The 6018-keV state also has the highest direct-capture cross section. In contrast, the extracted compound-nuclear cross section for the nearby 5936-keV state, which also has a high direct-capture component, is very small (see the last column of Table XVI).

If the large values of $\sigma_{\gamma(\mathrm{CN})}$ [given by the + sign of $\mp$ in Eq. (5)] are used for all except the 5936- and 6018-keV states, the mean value of $\sigma_{\gamma(\mathrm{CN})}/E_\gamma^3$ is 300×10^{-6} b MeV^{-3}, and the confidence level for the 6018-keV state is ~1%. If the large values of $\sigma_{\gamma(\mathrm{CN})}$ are used for all levels, the mean value is now 5400×10^{-6} b MeV^{-3}, and the confidence level for the 6018-keV state shrinks to ~0.2%. Even worse is to use the large $\sigma_{\gamma(\mathrm{CN})}$ value for the 5936-keV state and the small value for the 6018-keV state; this choice gives a mean value of 1600×10^{-6} b MeV^{-3}, and a confidence level for the 5936-keV state of ~0.1%. After discarding the scenarios that result in very low confidence levels, we conclude that (i) the average reduced compound-nuclear cross section is $\sim250\times10^{-6}$ b MeV^{-3}, (ii) the transition to the 5936-keV state is dominated almost completely by direct capture, and (iii) the transition to the 6018-keV state has a substantial component (~20% relative to direct) of compound-nuclear cross section. The rather low confidence level for this com-

ponent ($\sim$0.5%) would be improved if the (d,p) spectroscopic factors were to be raised. An increase of 20% across the board, within the accuracy of the experiment and theoretical analysis, would increase this confidence level to $\sim$1.5%.

Because the largest individual contribution to the average reduced compound-nuclear cross section comes from a transition to a final state with $J=2$, it appears that the principal level contributing to the compound-nuclear capture has $J=1$. From the average compound-nuclear capture cross section, we can deduce the radiation-width–energy-level relation from the equation

$$\langle \Gamma_{\gamma(\mathrm{CN})}/E_\gamma^3\rangle E_\lambda \approx k\langle \sigma_{\gamma(\mathrm{CN})}/E_\gamma^3\rangle/2\pi g R.\mathscr{R}_{\mathrm{loc}}, \qquad (6)$$

where k is the neutron wave number and g is the spin-weight factor of the initial state. The experimental value of this reduced width to energy ratio is about -110×10^{-9} MeV^{-3}. This value can be compared with Cameron's [107] semiempirical ratio of reduced width to mean level spacing (D),

$$\langle \Gamma_{\gamma(\mathrm{CN})}/E_\gamma^3\rangle/D \approx 0.33\times10^{-9}A^{2/3}\ \mathrm{MeV}^{-3}. \qquad (7)$$

Numerically, the Cameron estimate is 2.3×10^{-9} MeV^{-3} for ^{20}F. Comparison of the two numbers indicates that the binding of the initial state is about 1/50th of the mean level spacing ($\sim$300 keV).

In Sec. V A, we discussed evidence for the possible observation of a primary $M2$ transition in the (n,γ) reaction. The 4630.6-keV γ ray is very weak—only 6 ± 1 μb compared to the total capture cross section of 9.51 ± 0.09 mb. This $M2$ cross section value can be converted to a radiation width by comparison with the total compound-nuclear component ($\sim$1.3 mb) of the cross section (see Table XVI). The expected radiation width giving rise to this cross section is estimated from Cameron's relation to be $1.09\times10^{-6}D$. Using $D\approx300$ keV, we find a value of 0.33 eV for the total radiation width. The $M2$ cross section of 6 μb can therefore be attributed to a radiation width of $\sim$1.3 meV for this transition. The Weisskopf estimate for the 4630.6-keV γ ray is 0.25 meV if it is pure $M2$. The enhancement factor of $\sim$5 is at the very upper end of RUL for $M2$ transitions [79].

VII. SUMMARY

We have made a definitive study of the primary and secondary γ rays in ^{20}F following thermal-neutron capture by ^{19}F. Of the $\sim$88 known excited states in ^{20}F below the neutron separation energy, 36 were found to be populated in this reaction. For these states, we have determined accurate level energies and (whenever possible) γ-ray branching ratios. We have measured the lifetimes of 25 states in ^{20}F—several of these for the first time. We have distilled reliable spectroscopic information on low-lying levels from the vast literature on ^{20}F levels. This information has been compared with the results of an extensive shell-model calculation. The good overall agreement found between theory and experiment extends not only to the shell model as it pertains to the level properties, but also to the direct-capture theory, which is able to reproduce (within a factor of $\sim$2 for the five states with definite J^π assignments) the partial cross sections of the primary $E1$ transitions. A more conclusive comparison requires additional spectroscopic information, especially definite J^π assignments, for a greater number of levels above 2.8 MeV.

ACKNOWLEDGMENTS

This work was sponsored, in part, by the U.S. Department of Energy under Contract No. DE-AC05-84OR21400 with Lockheed Martin Energy Systems, Inc. (Oak Ridge), No. DE-AC02-76CH0016 with the Associated Universities, Inc. (Brookhaven), and No. W-7405-eng-36 with the University of California (Los Alamos), and, in part, by the Academy of Finland.

APPENDIX: EXAMPLE OF J^π AND MIXING-RATIO (δ^2) RESTRICTIONS FROM LIFETIMES AND γ-BRANCHING RATIOS

The 823-keV level has $\tau=79\pm6$ ps and branching ratios of (33.4 ± 3.3)% and (66.6 ± 3.3)%, respectively, for the 823$\rightarrow$0 keV and 823$\rightarrow$656 keV transitions (see Table VI). The partial lifetimes are

$$\tau_p(823\rightarrow0)=237\pm29\ \mathrm{ps} \qquad (A1a)$$

and

$$\tau_p(823\rightarrow656)=119\pm13\ \mathrm{ps}. \qquad (A1b)$$

To 3.3 standard deviations (that is, the 0.1% confidence limit), we have

$$\tau_p(823\rightarrow0)<\tau_p(0.1\%\mathrm{C.L.})=333\ \mathrm{ps} \qquad (A2a)$$

and

$$\tau_p(823\rightarrow656)<\tau_p(0.1\%\mathrm{C.L.})=155\ \mathrm{ps}. \qquad (A2b)$$

The Weisskopf estimates for these two transitions are

$$823\rightarrow0:\tau_{\mathrm{W.u.}}(E2)=671\ \mathrm{ps},$$

$$\tau_{\mathrm{W.u.}}(M2)=1.61\times10^4\ \mathrm{ps} \qquad (A3a)$$

and

$$823\rightarrow656:\tau_{\mathrm{W.u.}}(E2)=1.96\times10^6\ \mathrm{ps},$$

$$\tau_{\mathrm{W.u.}}(M2)=4.90\times10^7\ \mathrm{ps}. \qquad (A3b)$$

Then, from Eqs. (2a) and (2b), we have for the 823$\rightarrow$0 keV transition $|\delta(M2/E1)|<0.25$, and because RUL $\tau_p(0.1\%\mathrm{C.L.})$ exceeds the $E2$ Weisskopf estimate, there is no restriction on $|\delta(E2/M1)|$. For the 823$\rightarrow$656 keV transition, the restrictions are $|\delta(M2/E1)|<0.031$ and $|\delta(E2/M1)|<0.090$.

From these results we conclude that the 823-keV level must have $J^\pi=2^\pm,3^\pm$, or 4^+ with the restrictions on the mixing ratios given above. Using these mixing ratios, the angular-correlation measurements [27] rule out $J^\pi=2^-$ and $J^\pi=3^\pm$ at better than the 0.1% confidence limit. For $J^\pi=2^+$, the restriction on $\delta(E2/M1)$ for the 823$\rightarrow$0 keV

transition given by Longo *et al.* [24]—from a reanalysis of the data of Pronko and Nightingale [27]—is $-(2.5^{+4.5}_{-0.8})$. When used in the analysis of the linear-polarization measurement of the 823→0 keV transition [24], this restriction results in a rejection of the $J^\pi=2^+$ alternative at better than the 0.1% confidence limit, while a $J^\pi=4^+$ assignment to the 823-keV level with the 823→0 keV and 823→656 keV transitions being $E2$ and $M1+E2$, respectively, gives good agreement with all angular-correlation and linear-polarization data. Hence $J^\pi=4^+$.

[1] S. Raman, S. Kahane, and J. E. Lynn, in *Proceedings of the International Conference on Nuclear Data for Science and Technology, Mito, Japan, 1988,* edited by S. Igarasi (Saikon, Tokyo, 1988), p. 645; J. E. Lynn and S. Raman, in *Capture Gamma-ray Spectroscopy,* edited by R. W. Hoff, AIP Conf. Proc. No. 238 (AIP, New York, 1991), p. 555; S. Raman and J. E. Lynn, in *Beijing International Symposium on Fast Neutron Physics, Beijing, China, 1991,* edited by Sun Zuxun, Tang Hongqing, Xu Jincheng, and Zhang Jingshang (World Scientific, Singapore, 1992), p. 107.

[2] S. Raman, R. F. Carlton, J. C. Wells, E. T. Jurney, and J. E. Lynn, Phys. Rev. C **32**, 18 (1985).

[3] J. E. Lynn, S. Kahane, and S. Raman, Phys. Rev. C **35**, 26 (1987).

[4] S. Kahane, J. E. Lynn, and S. Raman, Phys. Rev. C **36**, 533 (1987); S. Raman, S. Kahane, R. M. Moon, J. A. Fernandez-Baca, J. L. Zarestky, J. E. Lynn, and J. W. Richardson, Jr., *ibid*. **39**, 1297 (1989); S. Raman, J. A. Fernandez-Baca, R. M. Moon, and J. E. Lynn, *ibid*. **44**, 518 (1991).

[5] J. E. Lynn, E. T. Jurney, and S. Raman, Phys. Rev. C **44**, 764 (1991).

[6] T. A. Walkiewicz, S. Raman, E. T. Jurney, J. W. Starner, and J. E. Lynn, Phys. Rev. C **45**, 1597 (1992).

[7] S. Raman, E. T. Jurney, J. W. Starner, and J. E. Lynn, Phys. Rev. C **46**, 972 (1992).

[8] M. C. Moxon, J. A. Harvey, S. Raman, J. E. Lynn, and W. Ratynski, Phys. Rev. C **48**, 553 (1993).

[9] F. Ajzenberg-Selove, Nucl. Phys. **A475**, 1 (1987).

[10] G.-B. Liu and H. T. Fortune, Phys. Rev. C **38**, 2134 (1988).

[11] J. C. Legg, D. J. Crozier, G. G. Seaman, and H. T. Fortune, Phys. Rev. C **18**, 2202 (1978).

[12] H. T. Fortune and J. N. Bishop, Nucl. Phys. **A293**, 221 (1977).

[13] H. T. Fortune and R. Eckman, Phys. Rev. C **31**, 2076 (1985).

[14] H. T. Fortune and J. N. Bishop, Nucl. Phys. **A304**, 221 (1978).

[15] A. A. Rollefson, P. F. Jones, and R. J. Shea, Phys. Rev. C **1**, 1761 (1970).

[16] H. T. Fortune, J. D. Garrett, J. R. Powers, and R. Middleton, Phys. Rev. C **4**, 850 (1971); **5**, 1438(E) (1972).

[17] D. J. Crozier and H. T. Fortune, Phys. Rev. C **10**, 1697 (1974).

[18] R. Medoff, L. R. Medsker, S. C. Headley, and H. T. Fortune, Phys. Rev. C **14**, 1 (1976).

[19] M. S. Chowdhury, M. A. Zaman, and H. M. Sen Gupta, Phys. Rev. C **46**, 2273 (1992).

[20] G. A. Bissinger, R. M. Mueller, P. A. Quin, and P. R. Chagnon, Nucl. Phys. **A90**, 1 (1967).

[21] P. A. Quin, A. A. Rollefson, G. A. Bissinger, C. P. Browne, and P. R. Chagnon, Phys. Rev. **157**, 991 (1967).

[22] P. A. Quin, G. A. Bissinger, and P. R. Chagnon, Nucl. Phys. **A155**, 495 (1970).

[23] L. A. Alexander, W. K. Collins, B. P. Hichwa, J. C. Lawson, D. S. Longo, E. D. Berners, and P. R. Chagnon, Phys. Rev. C **6**, 817 (1972).

[24] D. S. Longo, J. C. Lawson, L. A. Alexander, B. P. Hichwa, and P. R. Chagnon, Phys. Rev. C **8**, 1347 (1973).

[25] J. G. Pronko, Phys. Rev. C **7**, 127 (1973).

[26] D. P. Balamuth and E. G. Adelberger, Phys. Rev. C **16**, 928 (1977).

[27] J. G. Pronko and R. W. Nightingale, Phys. Rev. C **4**, 1023 (1971).

[28] P. Spilling, H. Gruppelaar, H. F. de Vries, and A. M. J. Spits, Nucl. Phys. **A113**, 395 (1968).

[29] R. Hardell and A. Hasselgren, Nucl. Phys. **A123**, 215 (1969).

[30] P. Hungerford, T. von Egidy, H. H. Schmidt, S. A. Kerr, H. G. Börner, and E. Monnand, Z. Phys. A **313**, 339 (1983).

[31] T. J. Kennett, W. V. Prestwich, and J. S. Tsai, Can. J. Phys. **65**, 1111 (1987).

[32] I. Bergqvist, J. A. Biggerstaff, J. H. Gibbons, and W. M. Good, Phys. Rev. **158**, B1049 (1967).

[33] M. J. Kenny, P. W. Martin, L. E. Carlson, and J. A. Biggerstaff, Aust. J. Phys. **27**, 759 (1974).

[34] A. A. Rollefson and J. A. Aymar, Phys. Rev. C **3**, 1704 (1971).

[35] H. T. Fortune, G. C. Morrison, R. C. Bearse, J. L. Yntema, and B. H. Wildenthal, Phys. Rev. C **6**, 21 (1972).

[36] H. T. Fortune and R. R. Betts, Phys. Rev. C **10**, 1292 (1974).

[37] C. A. Mosley, Jr. and H. T. Fortune, Phys. Rev. C **16**, 1697 (1977).

[38] P. A. Quin and S. E. Vigdor, Bull. Am. Phys. Soc. **15**, 1686 (1970).

[39] P. R. Chagnon, Nucl. Phys. **59**, 257 (1964).

[40] R. W. Newsome, Jr., Nucl. Phys. **71**, 353 (1965).

[41] R. L. Hershberger, M. J. Wozniak, Jr., and D. J. Donahue, Phys. Rev. **186**, 1167 (1969).

[42] T. Holtebekk, S. Tryti, and G. Vamraak, Nucl. Phys. **A134**, 353 (1969).

[43] K. A. Hardy and Y. K. Lee, Phys. Rev. C **7**, 1441 (1973).

[44] G. Scharff-Goldhaber, A. Goodman, and M. G. Silbert, Phys. Rev. Lett. **4**, 25 (1960).

[45] E. Freiberg and V. Soergel, Z. Phys. **162**, 114 (1966).

[46] D. E. Alburger, G. Wang, and E. K. Warburton, Phys. Rev. C **35**, 1479 (1987).

[47] N. M. Clarke, P. R. Hayes, M. B. Becha, C. N. Pinder, and S. Roman, J. Phys. G **16**, 1547 (1990); see also N. M. Clarke, S. Roman, C. N. Pinder, and P. R. Hayes, *ibid*. **19**, 1411 (1993).

[48] G. F. Millington, J. R. Leslie, W. McLatchie, G. C. Ball, W. G. Davies, and J. S. Forster, Nucl. Phys. **A228**, 382 (1974).

[49] G.-B. Liu and H. T. Fortune, Phys. Rev. C **37**, 1818 (1988).

[50] H. T. Fortune and J. D. Garrett, Phys. Rev. C **14**, 1695 (1976).
[51] R. J. Nickles, Nucl. Phys. **A134**, 308 (1969).
[52] T. Holtebekk, R. Strømme, and S. Tryti, Nucl. Phys. **A142**, 251 (1970).
[53] E. K. Warburton, J. W. Olness, G. A. P. Engelbertink, and T. K. Alexander, Phys. Rev. C **7**, 1120 (1973).
[54] E. K. Warburton, P. Gorodetzky, and J. A. Becker, Phys. Rev. C **8**, 418 (1973).
[55] H. P. Seiler, R. Kulessa, P. M. Cockburn, P. Marmier, and P. H. Barker, Nucl. Phys. **A241**, 159 (1975).
[56] R. L. Kozub, J. Lin, J. F. Mateja, C. J. Lister, D. J. Millener, J. W. Olness, and E. K. Warburton, Phys. Rev. C **27**, 158 (1983).
[57] J. Görres, J. Meissner, J. G. Ross, K. W. Scheller, S. Vouzoukas, M. Wiescher, and J. D. Hinnefeld, Phys. Rev. C **50**, R1270 (1994).
[58] A. H. Wapstra, Nucl. Instrum. Methods **292**, 671 (1990).
[59] S. F. Mughabghab, M. Divadeenam, and N. E. Holden, *Neutron Cross-Sections* (Academic, New York, 1981), Vol. 1, Part A, p. 1-1.
[60] J. Lindhard, M. Scharff, and H. E. Schiøtt, Mat. Fys. Medd. Dan. Vid. Selsk. **33**, No. 14 (1963).
[61] A. E. Blaugrund, Nucl. Phys. **88**, 501 (1966).
[62] D. C. Santry and R. D. Werner, Nucl. Instrum. Methods B **69**, 167 (1992).
[63] J. S. Forster, D. Ward, H. R. Andrews, G. C. Ball, G. J. Costa, W. G. Davies, and I. V. Mitchell, Nucl. Instrum. Methods **136**, 349 (1976).
[64] J. Keinonen, V. Karttunen, J. Räisänen, F.-J. Bergmeister, A. Luukkainen, and P. Tikkanen, Phys. Rev. B **34**, 8981 (1986).
[65] A. Kehrel, J. Keinonen, P. Haussalo, K. P. Lieb, and M. Uhrmacher, Radiat. Eff. Defects **118**, 297 (1991).
[66] P. Tikkanen, J. Keinonen, A. Kangasmäki, Zs. Fülöp, A. Z. Kiss, and E. Somorjai, Phys. Rev. C **47**, 145 (1993).
[67] J. Keinonen, in *Capture Gamma-ray Spectroscopy and Related Topics (Holiday Inn—World's Fair, Knoxville, Tennessee),* Proceedings of the Fifth International Symposium on Capture Gamma-ray Spectroscopy and Related Topics, edited by S. Raman, AIP Conf. Proc. No. 125 (AIP, New York, 1985), p. 557.
[68] P. Tikkanen, J. Keinonen, V. Karttunen, and A. Kuronen, Nucl. Phys. **A456**, 337 (1986).
[69] P. Tikkanen, J. Keinonen, R. Lappalainen, and B. H. Wildenthal, Phys. Rev. C **36**, 32 (1987).
[70] J. Keinonen, P. Tikkanen, A. Kuronen, A. Z. Kiss, E. Somorjai, and B. H. Wildenthal, Nucl. Phys. **A493**, 124 (1989).
[71] P. Tikkanen, J. Keinonen, K. Arstila, A. Kuronen, and B. H. Wildenthal, Phys. Rev. C **42**, 581 (1990).
[72] P. Tikkanen, J. Keinonen, A. Kuronen, A. Z. Kiss, E. Koltay, E. Pintye, and B. H. Wildenthal, Nucl. Phys. **A517**, 176 (1990).
[73] P. Tikkanen, J. Keinonen, A. Kangasmäki, Zs. Fülöp, A. Z. Kiss, and E. Somorjai, Phys. Rev. C **43**, 2162 (1991).
[74] E. J. Hoffman, D. M. van Patter, D. G. Sarantites, and H. J. Barker, Nucl. Instrum. Methods **109**, 3 (1973).
[75] J. F. Ziegler, J. P. Biersack, and U. Littmark, *The Stopping and Range of Ions in Matter* (Pergamon, New York, 1985), Vol. 1.
[76] P. Haussalo, J. Keinonen, U. M. Jäske, and J. Sievinen, J. Appl. Phys. **75**, 7770 (1994).
[77] J. Keinonen, A. Luukkainen, A. Anttila, and M. Erola, Nucl. Instrum. Methods **216**, 249 (1983).
[78] A. Kangasmäki, P. Tikkanen, and J. Keinonen, Phys. Rev. C **50**, 1370 (1994).
[79] P. M. Endt, At. Data Nucl. Data Tables **55**, 171 (1993).
[80] E. K. Warburton and B. A. Brown, Phys. Rev. C **46**, 923 (1992).
[81] E. K. Warburton, I. S. Towner, and B. A. Brown, Phys. Rev. C **49**, 824 (1994).
[82] B. H. Wildenthal, Prog. Part. Nucl. Phys. **11**, 5 (1984).
[83] B. A. Brown, A. Etchegoyen, W. D. M. Rae, and N. S. Godwin, computer code OXBASH, 1984 (unpublished).
[84] D. H. Glockner and R. D. Lawson, Phys. Lett. **53B**, 313 (1974).
[85] B. A. Brown and B. H. Wildenthal, Phys. Rev. C **28**, 2397 (1983); B. A. Brown and B. H. Wildenthal, At. Data Nucl. Data Tables **33**, 347 (1985); B. A. Brown, in *Proceedings of the International Nuclear Physics Conference, Harrogate, U.K., 1986,* edited by J. L. Durell, J. M. Irvine, and G. C. Morrison (Institute of Physics, Bristol, 1987), p. 119.
[86] D. J. Millener and E. K. Warburton, in *Nuclear Shell Models*, edited by M. Vallieres and B. H. Wildenthal (World-Scientific, Singapore, 1985), p. 365.
[87] E. K. Warburton and D. J. Millener, Phys. Rev. C **39**, 1120 (1989).
[88] B. S. Reehal and B. H. Wildenthal, Part. Nucl. **6**, 137 (1973).
[89] P. Descouvemont and D. Baye, Nucl. Phys. **A517**, 143 (1990); (private communication).
[90] K. Langanke, M. Wiescher, W. A. Fowler, and J. Görres, Astrophys. J. **301**, 629 (1986).
[91] S. Kubono, N. Ikeda, M. Yasue, T. Nomura, Y. Fuchi, H. Kawashima, S. Kato, H. Orihara, T. Shinozuka, H. Ohnuma, H. Miyatake, and T. Shimoda, Z. Phys. A **331**, 359 (1988); S. Kubono, H. Orihara, S. Kato, and T. Kajino, Astrophys. J. **344**, 460 (1989); S. Kubono, N. Ikeda, Y. Funatsu, M. H. Tanaka, T. Nomura, H. Orihara, S. Kato, M. Ohura, T. Kubo, N. Inabe, A. Yoshida, T. Ichihara, M. Ishihara, I. Tanihata, H. Okuno, T. Nakamura, S. Shimoura, H. Toyokawa, C. C. Yun, H. Ohnuma, K. Asahi, A. Chakrabarti, T. Mukhopadhyay, and T. Kajino, Phys. Rev. C **46**, 361 (1992); S. Kubono, Y. Funatsu, N. Ikeda, M. H. Tanaka, T. Nomura, H. Orihara, S. Kato, M. Ohura, T. Kubo, N. Inabe, T. Ichihara, M. Ishihara, I. Tanihata, H. Okuno, T. Nakamura, S. Shimoura, H. Toyokawa, C. C. Yun, H. Ohnuma, K. Asahi, A. Chakrabarti, T. Mukhopadhyay, and T. Kajino, Nucl. Instrum. Methods B **70**, 583 (1992).
[92] L. O. Lamm, C. P. Browne, J. Görres, S. M. Graff, M. Wiescher, A. A. Rollefson, and B. A. Brown, Nucl. Phys. **A510**, 503 (1990).
[93] M. S. Smith, P. V. Magnus, K. I. Hahn, A. J. Howard, P. D. Parker, A. E. Champagne, and Z. Q. Mao, Nucl. Phys. **A536**, 333 (1992).
[94] J. Görres, M. Wiescher, K. Scheller, D. J. Morrissey, B. M. Sherrill, D. Bazin, and J. A. Winger, Phys. Rev. C **46**, R833 (1992).
[95] B. A. Brown, A. E. Champagne, H. T. Fortune, and R. Sherr, Phys. Rev. C **48**, 1456 (1993).
[96] R. Coszach, Th. Delbar, W. Galster, P. Leleux, I. Licot, E. Liénard, P. Lipnik, C. Michotte, A. Ninane, J. Vervier, C. R. Bain, T. Davinson, R. D. Page, A. C. Shotter, P. J. Woods, D. Baye, F. Binon, P. Descouvemont, P. Duhamel, J. Vanhoren-

beeck, M. Vincke, P. Decrock, M. Huyse, P. Van Duppen, G. Vancraeynest, and F. C. Barker, Phys. Rev. C **50**, 1695 (1994).

[97] R. D. Page, G. Vancraeynest, A. C. Shotter, M. Huyse, C. R. Bain, F. Binon, R. Coszach, T. Davinson, P. Decrock, Th. Delbar, P. Duhamel, M. Gaelens, W. Galster, P. Leleux, I. Licot, E. Lienard, P. Lipnik, C. Michotte, A. Ninane, P. J. Sellin, Cs. Sükösd, P. Van Duppen, J. Vanhorenbeeck, J. Vervier, M. Wiescher, and P. J. Woods, Phys. Rev. Lett. **73**, 3066 (1994).

[98] A. Piechaczek, M. F. Mohar, R. Anne, V. Borrel, B. A. Brown, J. M. Corre, D. Guillemaud-Mueller, R. Hue, H. Keller, S. Kubono, V. Kunze, M. Lewitowicz, P. Magnus, A. C. Mueller, T. Nakamura, M. Pfützner, E. Roeckl, K. Rykaczewski, M. G. Saint-Laurent, W.-D. Schmidt-Ott, and O. Sorlin, Nucl. Phys. **A584**, 509 (1995).

[99] S. Raman, in *Proceedings of the Fourth International Symposium on Neutron-Capture Gamma-ray Spectroscopy and Related Topics, Grenoble, France, 1981,* edited by T. von Egidy, F. Gönnenwein, and B. Maier (Institute of Physics, Bristol, 1982), p. 357.

[100] J. Kopecky, Netherlands Energy Research Foundation Report No. ECN-99, 1981.

[101] W. V. Prestwich, M. A. Islam, and T. J. Kennett, Can. J. Phys. **69**, 855 (1991).

[102] A. P. Bogdanov, E. A. Rudak, A. V. Soroka, V. A. Tadeush, and F. I. Firsov, Yad. Fiz. **10**, 19 (1969) [Sov. J. Nucl. Phys. **10**, 17 (1970)].

[103] In new measurements, we find that the intensity of the putative $M2$ primary transition (capturing $\frac{1}{2}^+$ state $\rightarrow$ 174-keV, $\frac{5}{2}^-$ state) in ^{45}Ca is <0.15 mb, compared to an intensity of ~ 2.1 mb implied in Ref. [102].

[104] M. A. Lone, R. A. Leavitt, and D. A. Harrison, At. Data Nucl. Data Tables **26**, 511 (1981).

[105] H. T. Fortune and B. H. Wildenthal, Phys. Rev. C **30**, 1063 (1984).

[106] P. A. Moldauer, Nucl. Phys. **47**, 65 (1963).

[107] A. G. W. Cameron, Can. J. Phys. **37**, 322 (1959). Cameron's semiempirical expression for $E1$ radiation widths is based on experimental data between $A=30$ and $A=240$ and has a weak A dependence. In the absence of sound experimental data and analysis, it is generally assumed that Cameron's expression can be extrapolated to light nuclei.